Synergy of a STING agonist and an IL-2 superkine in cancer immunotherapy against MHC I–deficient and MHC I+ tumors

Natalie K. Wolf[a], Cristina Blaj[a,1], Lora K. Picton[b,c,d] 🔟, Gail Snyder[a,2], Li Zhang[a], Christopher J. Nicolai[a,3], Chudi O. Ndubaku[e,4], Sarah M. McWhirter[e,5], K. Christopher Garcia[b,c,d], and David H. Raulet[a,6] 🔟

Cyclic dinucleotides (CDN) and Toll-like receptor (TLR) ligands mobilize antitumor responses by natural killer (NK) cells and T cells, potentially serving as complementary therapies to immune checkpoint therapy. In the clinic thus far, however, CDN therapy targeting stimulator of interferon genes (STING) protein has yielded mixed results, perhaps because it initiates responses potently but does not provide signals to sustain activation and proliferation of activated cytotoxic lymphocytes. To improve efficacy, we combined CDN with a half life-extended interleukin-2 (IL-2) superkine, H9-MSA (mouse serum albumin). CDN/H9-MSA therapy induced dramatic long-term remissions of the most difficult to treat major histocompatibility complex class I (MHC I)–deficient and MHC I+ tumor transplant models. H9-MSA combined with CpG oligonucleotide also induced potent responses. Mechanistically, tumor elimination required CD8 T cells and not NK cells in the case of MHC I+ tumors and NK cells but not CD8 T cells in the case of MHC-deficient tumors. Furthermore, combination therapy resulted in more prolonged and more intense NK cell activation, cytotoxicity, and expression of cytotoxic effector molecules in comparison with monotherapy. Remarkably, in a primary autochthonous sarcoma model that is refractory to PD-1 checkpoint therapy, the combination of CDN/H9-MSA with checkpoint therapy yielded long-term remissions in the majority of the animals, mediated by T cells and NK cells. This combination therapy has the potential to activate responses in tumors resistant to current therapies and prevent MHC I loss accompanying acquired resistance of tumors to checkpoint therapy.

cancer immunotherapy | NK cell | T cell | IL-2 superkine | STING agonist

Recent advances in immunotherapy have vastly improved patient outcomes (1, 2). However, for most cancers, the majority of patients do not show clinical benefit. Most of the approved therapies are "checkpoint" therapies predicated on amplifying CD8+ T cell responses (1, 3). However, some tumors lack many neoantigens for T cell recognition (4, 5), or acquire defects in antigen presentation or major histocompatibility complex class I (MHC I) expression before or during therapy that confer resistance (6–10).

Natural killer (NK) cells kill cancer cells (11–14) and amplify adaptive immune responses (15–17) by recognizing stress-induced ligands (18, 19) and/or the absence of MHC class I on tumor cells (20–22). Their capacity to kill MHC I–deficient tumor cells, including those lacking neoantigens, suggests that mobilizing antitumor NK cells is an attractive approach to counteract evasion of T cell responses.

The cyclic guanosine monophosphate–adenosine monophosphate synthase–stimulator of interferon (IFN) genes (cGAS-STING) innate immune sensing pathway has shown promise in preclinical studies as a therapeutic target. The pathway is triggered by cytosolic DNA in mammalian cells (23), but can also be potently activated by exposure of cells to cyclic dinucleotides (CDNs) such as 2′,3′-cyclic guanosine monophosphate–adenosine monophosphate (cGAMP), an intermediate in the pathway that enters the cytosol of cells and binds and activates the STING protein (24–26). Activated STING in turn activates both the IFN-regulatory factor 3 (IRF3) and nuclear factor κB (NF-κB) pathways, leading to production of type I IFNs and other inflammatory cytokines and chemokines (27). The same pathway is activated naturally, but probably quite weakly, in many tumors due to the escape of nuclear or mitochondrial DNA to the cytosol in cancer cells (28, 29).

Synthetic CDNs serve as potent STING agonists that, when injected intratumorally (i.t.) or systemically, superactivate antitumor T cell responses (30, 31). Similarly, we recently demonstrated that i.t. injections of CDNs induce robust NK cell–mediated rejection of six different established MHC I–deficient murine tumors, generated by CRISPR-Cas9 disruption of the *B2m* gene in each line (32). The CDN injections induced high levels of type I IFN, which was essential for NK cell activation, and acted directly on NK

Significance

Immunotherapy provides long-term remissions in numerous types of cancer but is ineffective in most tumors with poor immune cell infiltrates or lacking T cell epitopes or MHC I molecules. Agents that activate the STING protein showed promise in several MHC I+ and MHC-deficient tumor models in mice, where they induced powerful antitumor CD8+ T cell and natural killer (NK) cell responses, respectively. They were less effective in numerous other tumor models and yielded mixed results in the clinic in human patients. This report demonstrates strong synergy between a STING agonist and an IL-2 superkine in effectively curing difficult-to-treat MHC-deficient and MHC-positive tumor models in mice by mobilizing T cells and NK cells. This combination therapy shows considerable promise for clinical application.

[1]Present address: REVOLUTION Medicines, Redwood City, CA 94063.

[2]Present address: Department of OHNS, Head & Neck Surgery Division, Stanford University School of Medicine, Stanford, CA 94305.

[3]Present address: Umoja Biopharma, Seattle, WA 98101.

[4]Present address: Drug Discovery, ORIC Pharmaceuticals, South San Francisco, CA 94080.

[5]Present address: Biology Department, Lycia Therapeutics, South San Francisco, CA 94080.

[6]To whom correspondence may be addressed. Email: raulet@berkeley.edu.

cells and indirectly by inducing *trans*-presentation of IL-15 by dendritic cells (DCs). We observed permanent remissions of >50% of tumors in four of the six MHC I–deficient models studied. In two models, the rate of permanent remissions was much lower: ~20% in the MC38-*B2m*$^{-/-}$ model and 0% in the B16-F10-*B2m*$^{-/-}$ model (32). At the same time, early-phase clinical trials of STING agonists in patients have not yielded sustained clinical remissions (33, 34), indicating a need for improvements in this immunotherapy approach.

Superkines are an emerging category of immunotherapy agents that powerfully activate immune cells. The superkine H9, also known as super-2, is a variant of interleukin-2 (IL-2) that was selected to bind with high affinity to the IL-2Rβ/γ complexes that NK cells express (35). H9 activates NK cells at much lower concentrations than IL-2, and was shown to stimulate antitumor responses in mouse tumor models with lower toxicity than IL-2 (35). Furthermore, H9 administration reversed or delayed the onset of NK cell desensitization and prolonged the survival of mice with MHC-deficient tumors, in an NK cell–dependent fashion (36). Because STING agonists provide a potent initial stimulus for NK cell responses but may not provide continual cytokine production to sustain the responses, we evaluated the combination of a STING agonist with repeated administrations of the H9 superkine to sustain effective NK cell responses against cancer, in both tumor transfer models and primary cancers. The results demonstrate remarkable efficacy of this combination therapy in both MHC I–deficient and MHC I$^+$ tumor models.

Results

Half Life–Extended IL-2 Superkine, H9, Synergized with CDNs to Induce Rejection of MHC Class I–Deficient Tumors.

Injections of the STING agonist ADU-S100 (mixed-linkage [2′,3′] dithio-(Rp, Rp) cyclic diadenosine monophosphate, hereafter referred to as CDN) i.t. resulted in long-term tumor regressions in the majority of animals in four of the six MHC I–deficient (*B2m*$^{-/-}$) tumor models previously tested. Poor efficacy was observed in two models, the B16-F10-*B2m*$^{-/-}$ melanoma model (no long-term survivors) and the MC38-*B2m*$^{-/-}$ colorectal cancer model (~20% long-term survivors). In order to sustain the initial response in difficult-to-treat models, we combined CDN therapy with administration of the H9 superkine. Like IL-2, H9 has a short half-life in vivo. To extend the half-life and reduce toxicity due to high-dose administration, H9 was fused to mouse serum albumin (MSA) (37) to create H9-MSA. Monotherapy with repeated doses of 5 or 20 μg H9-MSA slowed tumor growth and extended survival of the tumor-bearing mice to a similar extent, resulting in long-term survival of ~20% of the animals. In contrast, H9 by itself had no significant antitumor activity (*SI Appendix*, Fig. S1A).

In the same tumor model, a single i.t. injection of CDN also slowed tumor growth, but combining CDN with 10- or 20-μg doses of H9-MSA provided dramatically improved outcomes, resulting in long-term (>100 d) tumor-free survival in 75 to 85% of the mice (Fig. 1 A and B and *SI Appendix*, Figs. S1B and S2A). CDN combined with H9 (lacking MSA) was less efficacious, and CDN combined with IL-2 was little better than CDN alone (*SI Appendix*, Fig. S1C).

The CDN/H9-MSA combination was even more effective in the MC38-*B2m*$^{-/-}$ model, resulting in long-term tumor-free remissions in 100% of the animals (Fig. 1C and *SI Appendix*, Fig. S2B). Treatments with CDN or H9-MSA alone were much less effective (Fig. 1C and *SI Appendix*, Fig. S2B). Thus, the combination of STING agonist and half life–extended H9

superkine was extremely effective in eliminating tumors in two very difficult to treat MHC I–deficient murine cancer models.

The combination of CDN (one treatment) and 10 μg H9-MSA (every 2 d) resulted in modest weight loss and a minor increase in lung/body weight ratio, a metric for pulmonary edema, a known side effect of IL-2 therapy (38) (*SI Appendix*, Fig. S3). Greater weight loss and pulmonary edema were associated with the 20-μg dose of H9-MSA by itself. CDN alone had the least toxicity in all tests performed, corresponding to transient weight loss that in a separate experiment was maximal on day 1. Administering 10 μg H9-MSA every 3 d further minimized toxicity while maintaining efficacy, and we employed that dose and schedule for most of the experiments in this study.
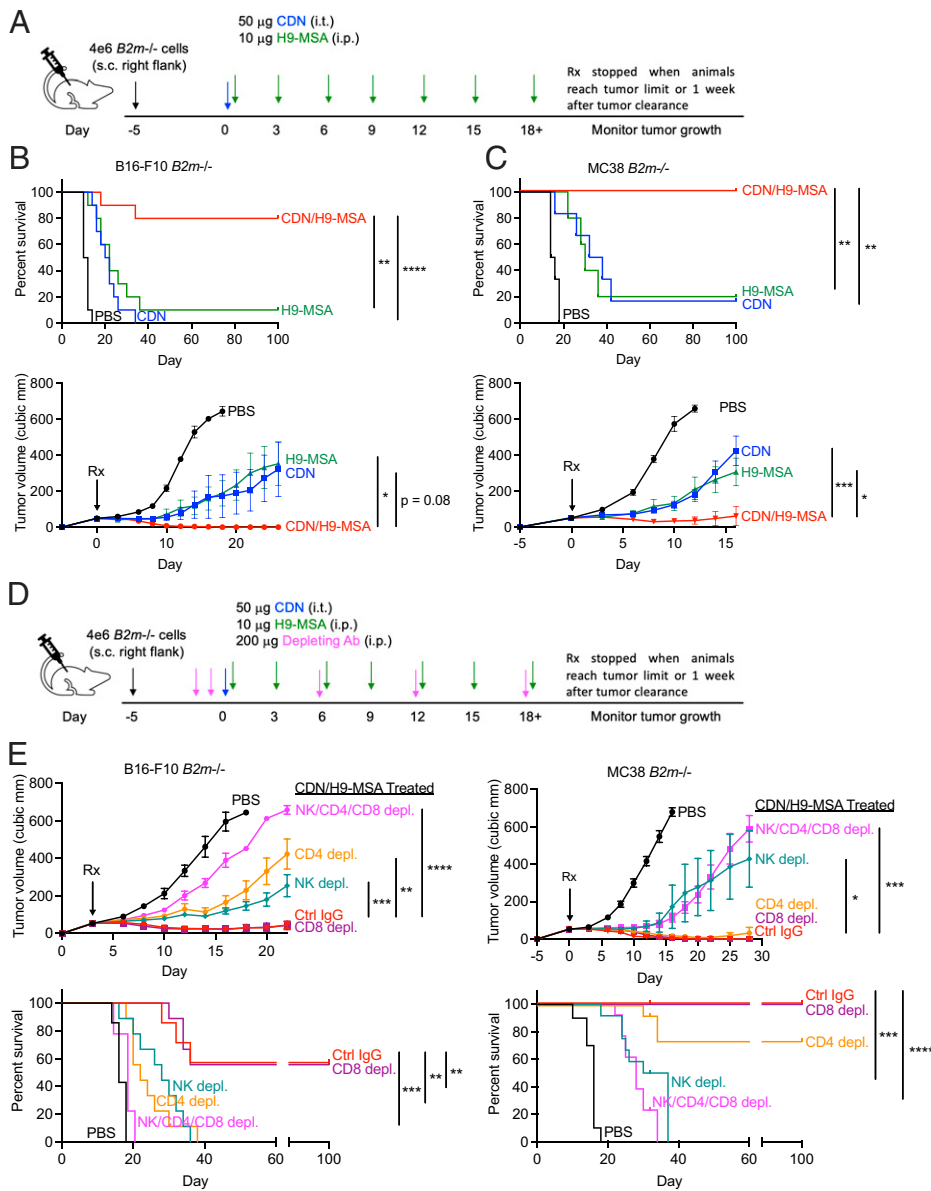
Rejection of MHC I–Deficient Tumors Induced by CDN/H9-MSA Therapy Was NK Cell Dependent and CD8 T Cell Independent.

In the MC38-*B2m*$^{-/-}$ model, depleting either CD4$^+$ or CD8β$^+$ cells starting after tumors were established but just before therapy was initiated (Fig. 1D and *SI Appendix*, Fig. S4) did not significantly diminish efficacy, whereas depleting NK cells alone greatly diminished therapeutic efficacy, resulting in terminal morbidity of all the animals (Fig. 1E and *SI Appendix*, Fig. S2D). Depleting all three types of lymphocytes had no greater effect than depleting NK cells. Therefore, NK cells, and not CD4 or CD8 T cells, mediate tumor rejection.

In the B16-F10-*B2m*$^{-/-}$ model, depleting CD8 T cells had no effect, but depleting either NK cells or CD4 T cells diminished therapeutic efficacy (Fig. 1E and *SI Appendix*, Fig. S2C). Depleting all three populations had an even greater effect, suggesting that combination therapy separately mobilized both antitumor NK cells and antitumor CD4 T cells, and that each acted to some extent independently. Antitumor CD4 T cells were previously implicated as antitumor effector cells in studies of wild-type (WT) B16 tumors (39, 40).

To address whether nonconventional T cells or B cells were necessary for tumor rejection, we tested the combination therapy in tumor-bearing B6-*Rag2*$^{-/-}$ mice, which lack all T cells (including NK1.1$^+$ T cells) and B cells but retain NK cells. In both tumor models, CDN and H9-MSA were more potent in combination than separately in the B6-*Rag2*$^{-/-}$ mice (Fig. 2). In the MC38-*B2m*$^{-/-}$ model, the combination therapy was as effective in *Rag2*$^{-/-}$ mice as in WT mice, resulting in 100% survival of the mice (Fig. 2 A and C and *SI Appendix*, Fig. S5A). As before, NK depletion greatly diminished efficacy, resulting in 100% mortality. In the B16-F10-*B2m*$^{-/-}$ model, combination therapy only delayed tumor growth in *Rag2*$^{-/-}$ mice, and 100% of the animals eventually succumbed (Fig. 2 B and D and *SI Appendix*, Fig. S5B). This finding is consistent with the data showing that CD4 cell depletion greatly diminished the rejection of these tumor cells in WT mice (Fig. 1B). NK depletion in *Rag2*$^{-/-}$ mice accelerated tumor growth, as expected. Thus, combination therapy mobilized a fully effective antitumor NK response against MC38-*B2m*$^{-/-}$ tumors, with no discernable role for conventional or nonconventional T cells. In contrast, both antitumor NK cells and antitumor CD4 T cells participated in rejecting B16-*B2m*$^{-/-}$ tumors in WT mice, albeit to a significant extent independently. Separately, each effector cell type delayed tumor growth but did not eliminate the tumors, but together they eliminated the tumors in most animals. There was no indication of a role for nonconventional T cells in elimination of B16-*B2m*$^{-/-}$ tumor cells, since the defect in tumor rejection in *Rag2*$^{-/-}$ mice was similar to the defect in WT mice depleted of CD4 T cells. CD8 T cells played no discernable role in either response.

Some delay in tumor growth was still evident after depleting all three lymphocyte populations in both tumor models (Fig. 1) and

Fig. 1. Cell types mediating rejection of MHC I–deficient tumors induced by CDN combined with the IL-2 superkine, H9-MSA. (A) Timeline. Tumor cells were implanted s.c. in C57BL/6J mice and grown to ~50 mm³ (day 0). Tumors were injected once i.t. with 50 µg of CDN or PBS. Mice were also injected i.p. with 10 µg of H9-MSA or PBS on day 0 and repeated every 3 d until euthanization or 1 wk after tumor clearance. (B and C) Tumor growth curves and survival of mice with B16-F10-$B2m^{-/-}$ (B) and MC38-$B2m^{-/-}$ (C) tumors. (D) Timeline for cellular depletions. Tumors were established and treated as in A, except groups of mice were depleted of NK cells, CD8 T cells, and/or CD4 T cells, or injected with control IgG. (E) Tumor growth curves and survival of mice with B16-F10-$B2m^{-/-}$ (Left) and MC38-$B2m^{-/-}$ (Right) tumors. Tumor growth data were analyzed by two-way ANOVA. Survival data were analyzed using log-rank (Mantel– Cox) tests. The data are representative of at least two independent experiments. $n = 7$ to 10 mice per group. Error bars represent standard error of the mean (SEM). *$P < 0.05$, **$P < 0.01$, ***$P < 0.001$, ****$P < 0.0001$.

in the $Rag2^{-/-}$ tumor models following NK cell depletion (Fig. 2). This delay was partially prevented by simultaneously blocking tumor necrosis factor α (TNF-α) and type I IFN receptors (Fig. 3A), suggesting that these cytokines impeded tumor growth independent of CD4, CD8, and NK cells after CDN/H9-MSA therapy, consistent with published reports (31, 32, 41). Blocking either TNF-α or type I IFN receptors separately (Fig. 3B) also showed a significant increase in tumor growth, indicating that these cytokines each played a separate, if minor, role in impeding tumor growth. However, some slowing of tumor growth was still apparent when blocking the cytokines in the absence of T cells and NK cells, suggesting that an unidentified mechanism also plays a role.

H9-MSA Was More Effective than WT IL-2-MSA in Combination with CDNs. We next directly compared H9-MSA with WT IL-2-MSA in the context of the combination therapy in WT mice with established B16-$B2m^{-/-}$ tumors. The mice were depleted of CD4 and CD8 T cells before the initiation of therapy to narrow the analysis to the effects of NK cells. The CDN/H9-MSA combination was again more effective than CDN or H9-MSA alone (Fig. 4A). The CDN/IL-2-MSA combination, in contrast, was only slightly more effective than CDN or IL-2-MSA alone

(Fig. 4B). In the head-to-head comparison, the CDN/H9-MSA combination was more effective than the CDN/IL-2-MSA combination, both in terms of delaying tumor growth and delaying terminal morbidity (Fig. 4C and SI Appendix, Fig. S6A). Therefore, H9-MSA is more effective than IL-2-MSA in activating NK cells against B16-$B2m^{-/-}$ tumors.

A Distinct Innate Activator, CpG Oligonucleotide, Also Synergized with H9-MSA in Providing Antitumor Efficacy. The Toll-like receptor 9 (TLR9) ligand CpG oligodeoxynucleotide (ODN), like CDNs, induces production of IFNs and other cytokines downstream of IRF3 and NF-κB. Similar to our findings with CDN (Fig. 4D), combining H9-MSA (intraperitoneally, i.p.) with CpG ODN (administered once, i.t.) resulted in delayed tumor growth and extended survival in mice that had been depleted of CD4 and CD8 T cells (Fig. 4E and SI Appendix, Fig. S6B). These findings indicated that at least two IFN-inducing innate agonists, CDN and CpG ODN, show synergistic effects with H9-MSA.

Local CDNs and Systemic H9-MSA Synergized in Creating a Systemic NK Cell–Mediated Antitumor Effect. To address whether CDN/H9-MSA therapy induces a systemic NK cell
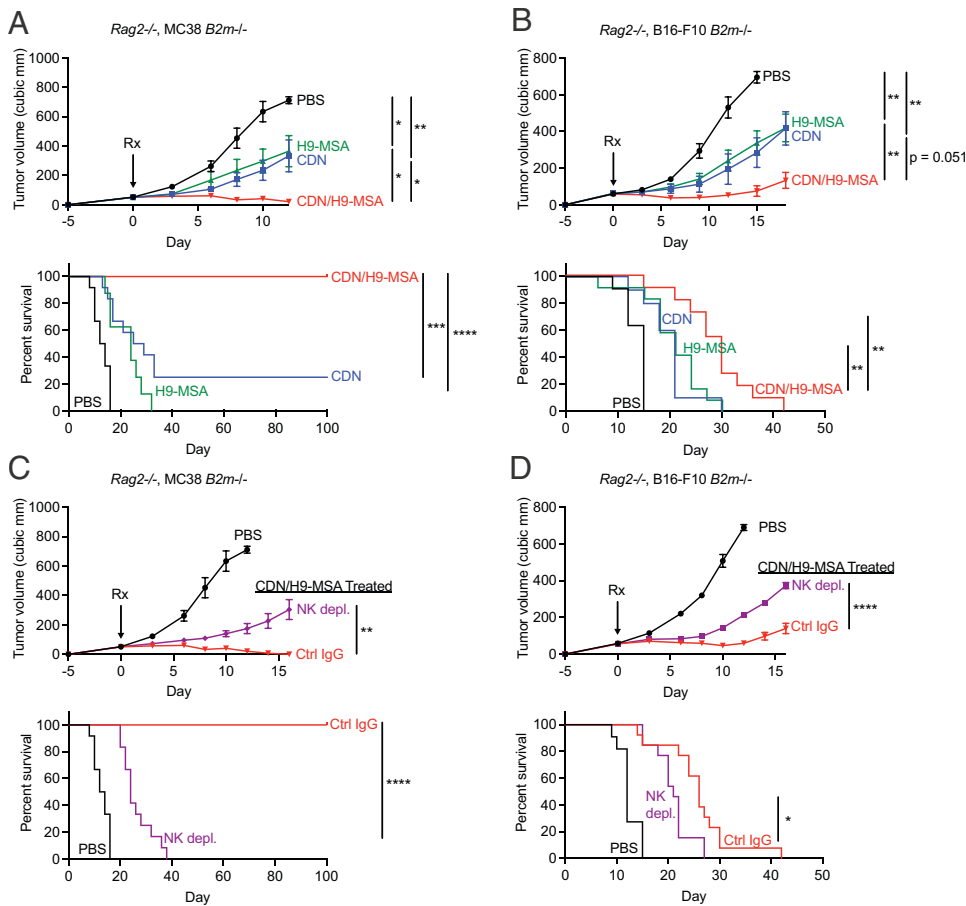
Fig. 2. NK cell–dependent rejection of MHC I–deficient tumors induced by CDN/H9-MSA treatment in $Rag2^{-/-}$ mice. MC38-$B2m^{-/-}$ (A and C) and B16-F10-$B2m^{-/-}$ (B and D) tumors were established as in the Fig. 1 legend in $Rag2^{-/-}$ mice, and subjected to therapy as indicated. (A and B) Combination therapy was more effective than monotherapies in both tumor models. (C and D) The therapeutic effects were decreased by NK depletion in both models. Tumor growth data were analyzed by two-way ANOVA. Survival data were analyzed using log-rank (Mantel–Cox) tests. The data are representative of at least two independent experiments. $n = 9$ to 12 mice per group. Error bars represent standard error of the mean (SEM) . $*P < 0.05$, $**P < 0.01$, $***P < 0.001$, $****P < 0.0001$.

effect with the potential to reject metastases, we established a bilateral tumor model system. B16-F10-$B2m^{-/-}$ tumors were established on both flanks of syngeneic mice (Fig. 5A). In order to focus on the NK-mediated effect, all the mice were depleted of CD4 and CD8 T cells before the start of treatment. Tumors on the right flank of each mouse were injected with either phosphate-buffered saline (PBS) or CDN. H9-MSA or PBS was then delivered intraperitoneally. As before, combination therapy was more effective than the single therapies in the CDN-injected tumors (Fig. 5B and SI Appendix, Fig. S7A). Remarkably, the same was true in the contralateral tumors that were not injected with CDN, corroborating that local CDN therapy by itself exerted a systemic effect (32) and demonstrating that CDN synergized with H9-MSA in mobilizing greater systemic antitumor effects (Fig. 5B and SI Appendix, Fig. S7A). Depletion of NK cells diminished the efficacy of combination therapy similarly in both the injected tumor and the uninjected tumor (Fig. 5C and SI Appendix, Fig. S7). As these mice were depleted of CD4 and CD8 T cells, the data implicated NK cells as major antitumor effectors both locally and in the distant tumor. Some delay in tumor growth in both tumors was still evident after simultaneous depletion of NK cells and CD4 and CD8 cells. Part of the residual effects of therapy in these conditions may be due to systemic TNF and IFN, based on the findings within single-tumor experiments (Fig. 3).

CDN/H9-MSA Combination Therapy Mobilized More Activated Intratumoral NK Cells with Greater Functional Activity. To address the mechanisms underlying the synergy of CDN and H9-MSA in induction of antitumor NK cell responses, we employed the bilateral tumor system and examined markers of

activation on NK cells infiltrating both tumors 2 and 5 d after treatment. The percentages of granzyme B^+ NK cells in the tumors, and the levels of granzyme B per cell (mean fluorescence intensity of staining), were significantly elevated in mice treated with CDN/H9-MSA compared with mice treated with CDN alone (on day 5 for both injected and uninjected tumors), or compared with mice treated with H9-MSA alone (levels of granzyme B per cell on day 2 for uninjected tumors and on day 5 for injected tumors) (Fig. 6 A and B and SI Appendix, Figs. S8 and S9). The percentages of $CD69^+$ NK cells in the tumors were significantly elevated in mice treated with CDN/H9-MSA compared with mice treated with CDN alone (on day 5, and in uninjected tumors on day 2), or compared with mice treated with H9-MSA alone (on day 2) (Fig. 6 A and B and SI Appendix, Figs. S8 and S9). The percentages of NK cells expressing the activation marker Sca1 were also elevated in mice receiving combination therapy compared with mice receiving CDN therapy, and in uninjected tumors compared with mice receiving H9-MSA therapy (SI Appendix, Fig. S10 A and B). On day 2, the percentages of NK cells among $CD45^+$ cells were elevated in uninjected tumors in mice receiving combination therapy compared with mice receiving CDN therapy (Fig. 6 A and B and SI Appendix, Figs. S8 and S9). Overall, the combination therapy elicited NK cells showing higher levels of activation or granzyme B expression than did the individual therapies.

The greater activity of NK cells after combination therapy was evident when cytotoxic activity of splenic NK cells was tested ex vivo, despite there being no significant increase in NK cell numbers in the spleen (SI Appendix, Fig. S11). The lysis of B16-F10-$B2m^{-/-}$ tumor cells by splenic NK cells was highly
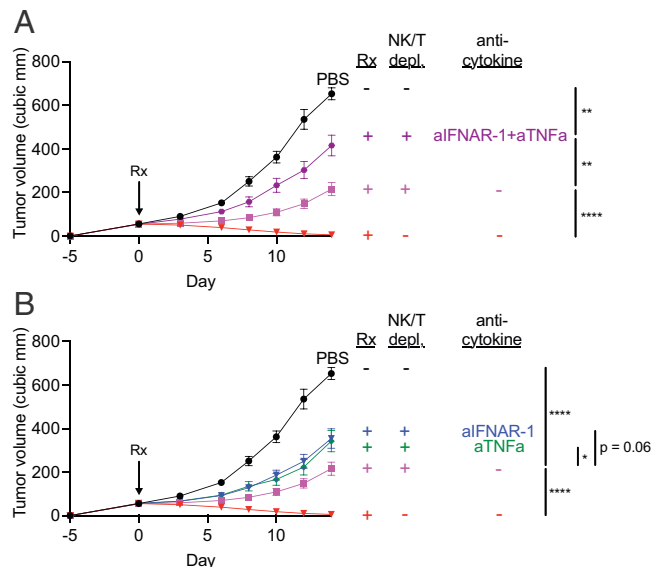
Fig. 3. Blockade of TNF-α and IFNAR-1 partially reverses the tumor growth delay imparted by CDN/H9-MSA administration in mice depleted of T cells and NK cells. B16-F10-*B2m*$^{-/-}$ tumors were generated and mice received therapy as described in the Fig. 1 legend. Mice were depleted of NK cells, CD4 T cells, and CD8 T cells i.p. on days −2 and −1 before the initiation of therapy and repeated every 6 d. Additionally, mice received anti–IFNAR-1 and/or anti–TNF-α i.p. on day −1 and day 0 before the initiation of therapy and again every 3 d. Blockade of TNF-α and IFNAR-1 (A) or blockade of TNF-α or IFNAR-1 (B) led to more rapid tumor growth in the NK/T cell–depleted animals. Tumor growth data were analyzed by two-way ANOVA. The data are a combination of two experiments. *n* = 10 or 11 mice per group. Panel A and B are from the same experiments but separated for clarity. Error bars represent standard error of the mean (SEM). *P < 0.05, **P < 0.01, ****P < 0.0001.

elevated 24 or 72 h after initiating treatment with the combination therapy, and was more sustained compared with separate treatments with CDN or H9-MSA (Fig. 6C). NK depletion abrogated killing as expected (Fig. 6D). In parallel, the percentages of splenic NK cells showing elevated granzyme B, CD69, or Sca1 were significantly elevated in mice two days after receiving the combination therapy compared with mice receiving the separate therapies (*SI Appendix*, Fig. S10 *C* and *D*). These data demonstrated that the combination therapy had multiple impacts, maximizing NK cell activation and content of cytotoxic effector molecules (granzyme B), as well as cytotoxicity, and prolonging the NK response compared with each therapy separately.

CDN/H9-MSA Therapy Mobilized CD8 T Cells against MHC I$^+$ Tumors. The impact of combination therapy on NK cell–dependent tumor rejection prompted us to ask whether this approach has broader applicability, including against MHC I$^+$ tumors. Therefore, we tested whether the CDN/H9-MSA therapy combination is effective with "wild-type" MHC I$^+$ B16-F10 tumors, a model that is poorly responsive to most therapies including checkpoint therapy. B6 mice with established MHC I$^+$ B16-F10 tumors treated separately with CDN or H9-MSA showed delays in tumor growth but very poor long-term survival, whereas the combination of CDN/H9-MSA showed synergistic tumor rejection and disease-free survival of most of the mice for >100 d (Fig. 7A and *SI Appendix*, Fig. S12A).

Cell depletion experiments demonstrated that CD8 T cells were essential for rejection of the MHC I$^+$ tumors, whereas CD4 cells and NK cells were largely dispensable (Fig. 7B and *SI Appendix*, Fig. S12B). Elimination of all three populations

was no more impactful than CD8 depletion alone. Thus, CD8 T cells are very effectively mobilized against MHC I$^+$ tumors by this combination therapy. Thus, combining an innate agonist and IL-2 superkine synergistically mobilized T cells or NK cells against tumors, depending on the MHC expression status of the tumor cells.

Efficacy of Combination Therapy in the Methylcholanthrene-Induced Sarcoma Model. Subcutaneous (s.c.) tumor models are generally easier to treat than autochthonous tumor models, which are more similar to human cancers. To address the efficacy of the CDN/H9-MSA combination in a primary autochthonous cancer model, we chose the methylcholanthrene (MCA)-induced sarcoma model. MCA was injected s.c. on the right flanks and mice were monitored frequently for palpable tumors, which arose 8 to 10 wk after carcinogen administration in 80% of the treated animals. When a tumor reached a volume of ~50 mm^3, the mouse was treated individually. Mice were initially injected with three doses of CDN i.t. every 3 d followed by weekly injections. Some mice received H9-MSA i.p. applied every 3 d (Fig. 7C). H9-MSA alone had a minor, albeit significant effect on tumor growth and terminal morbidity of the animals, whereas CDN therapy caused a substantial delay in both tumor progression and terminal morbidity (Fig. 7D and *SI Appendix*, Fig. S13A). The CDN/H9-MSA combination was significantly more effective than CDN alone in prolonging survival, with a small percentage of animals surviving after 160 d.

Some toxicity of the CDN/H9-MSA combination was evident in this model, including the appearance of chronic granulomatous histiocytic inflammation in some mice, that arose in the leg muscle on the same side of the mouse as the treated tumor. When treated with topical diphenhydramine (Benadryl), the inflammation was partially controlled, and mice continued in the experiment.

The initial antitumor effects were significantly diminished when either NK cells, CD8 cells, or, to a lesser extent, CD4 cells were depleted from the animals before initiating therapy (Fig. 7E and *SI Appendix*, Fig. S13B). Depleting NK cells accelerated the demise of a fraction of the animals, whereas depleting CD8 or CD4 cells accelerated the demise of all the animals. Depleting all three populations simultaneously had a modestly greater effect than depleting CD8 or CD4 cells separately, suggesting some separate impacts of these lymphocyte populations, though some cooperative interactions between the populations are fully consistent with the data. Thus, NK cells, CD8 T cells, and CD4 T cells all contribute to the therapeutic effects in this tumor model.

Although the CDN/H9-MSA combination showed efficacy in treating primary MCA tumors, nearly all the mice eventually succumbed. Therefore, we tested whether efficacy could be improved by adding checkpoint therapy to the combination. Addition of anti–PD-1 therapy did not result in an improvement in survival, nor did addition of anti-TIGIT therapy (Fig. 7F and *SI Appendix*, Fig. S13C). However, simultaneous blockade of PD-1 and TIGIT, in combination with CDN/H9-MSA, was significantly more effective than CDN/H9-MSA therapy alone (Fig. 7F and *SI Appendix*, Fig. S13C). When all four components were injected simultaneously, we observed instances of severe, in some cases fatal, toxicity. We found that delaying the anti-TIGIT treatments by 1 d greatly ameliorated that toxicity. Therefore, we subsequently incorporated delayed anti-TIGIT treatments into our treatment regimen for analysis of additional animals. Notably, in mice that received the four-
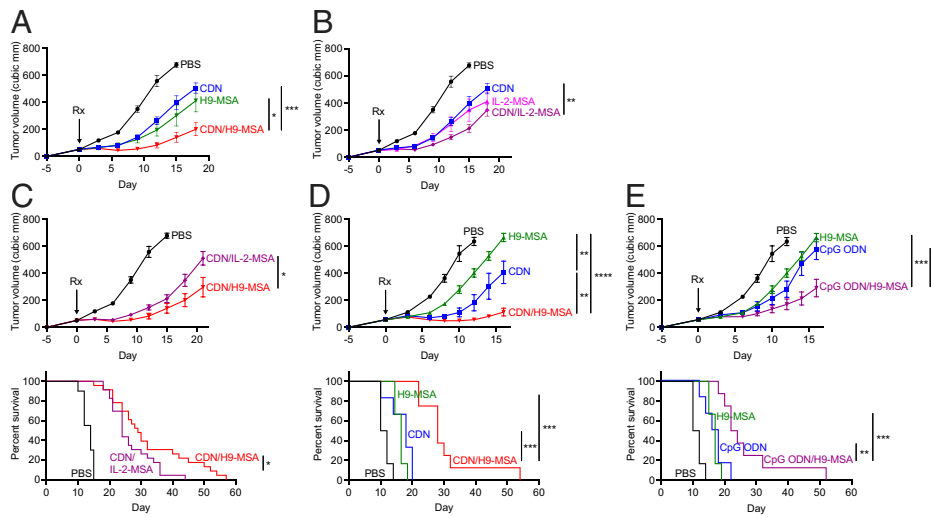
Fig. 4. Greater efficacy of H9-MSA compared with IL-2-MSA in mice lacking CD4 and CD8 T cells, and synergy of CpG ODN and H9-MSA. B16-F10-$B2m^{-/-}$ tumors were established as in the Fig. 1 legend in C57BL/6J mice. In all panels, the mice were depleted of both CD4 and CD8 T cells before initiating therapy. (*A–C*) Comparisons of the effects of CDN, H9-MSA, and IL-2-MSA separately (*A* and *B*) or in combination (CDN/IL-2-MSA vs. CDN/H9-MSA) (*A–C*) using the schedule shown in Fig. 1, with one dose of 50 µg of CDN and 10-µg doses of H9-MSA or IL-2-MSA. Curves in *A–C* are all from the same experiment. (*D* and *E*) Comparison of the effects of CDN, CpG ODN, and H9-MSA separately or in combination (CDN/H9-MSA vs. CDN/CpG ODN/H9-MSA). Curves in *D* and *E* are from the same experiment. Tumor growth data were analyzed by two-way ANOVA. Survival data were analyzed using log-rank (Mantel–Cox) tests. The data are representative at least two independent experiments. $n = 9$ to 20 mice per group. Error bars represent standard error of the mean (SEM). *$P < 0.05$, **$P < 0.01$, ***$P < 0.001$, ****$P < 0.0001$.

component therapy regimen, 44% of the animals (8/18) survived tumor-free for >160 d. Interestingly, the chronic inflammation noted in some mice treated with CDN/H9-MSA was not observed in the mice receiving all four agents. Mice that received anti–PD-1 or anti-TIGIT treatments alone or together did not show prolonged survival (*SI Appendix*, Fig. S13D). CDN therapy outcomes were also not improved by the addition of anti–PD-1 or anti-TIGIT separately (*SI Appendix*, Fig. S13E). In conclusion, simultaneous blockade of PD-1 and TIGIT was necessary to unleash a fully effective antitumor immune response initiated by CDN/H9-MSA treatments.

Discussion

The CDN/H9-MSA therapy combination synergistically induced profound antitumor responses in several solid tumor models, including MHC I–deficient and MHC I⁺ tumor transplant models. The combination was also effective for treating primary MCA-induced sarcomas, although in that model long-term survival was less frequent and depended on concomitant checkpoint therapy. The success of the combination in this autochthonous model is encouraging, however, because it is very difficult to cure and likely mimics human cancer better than s.c. tumors. We suspect that the therapy combination would be very effective for hematologic malignancies as well, considering that such tumor cells are frequently highly sensitive to NK cell–mediated killing. It remains to be seen whether this therapy combination will be effective for larger tumors than tested here.

An important consideration for clinical applications is whether therapies elicit control of metastases distant from the site of a primary tumor, which are known to limit the efficacy of immunotherapies (42, 43). We observed that local administration of CDN in a primary tumor, combined with systemic applications of H9-MSA, resulted in strong systemic activation of NK cells capable of limiting the growth of a second tumor on the opposite flank of the animals and mediating killing of tumor cells in ex vivo tests with splenic NK cells. In contrast, NK cell activation after a single treatment with CDN alone was short-lived, as by 72 h after treatment, cytotoxicity by splenic NK cells had subsided. Thus, the combination therapy sustained the systemic cytotoxicity of NK cells. We suspect that the impact of i.t. injections of CDN on NK cell activation in a distant second tumor or in the spleen is due to induced accumulation of systemic IFN which resulted in >1 ng/mL IFNβ

detected in the serum after i.t. CDN injections in a different tumor model (32). Systemic accumulation of other cytokines induced by i.t. CDN injections and/or the leakage of small amounts of CDN from the tumor into the general circulation (31) may also play a role. We think it is unlikely that the systemic effects are due to trafficking of NK cells activated at the site of treatment to other sites, because the percentage of activated NK cells in uninjected tumors was close to 100% as assessed by Sca1 expression (*SI Appendix*, Fig. S10 *A* and *B*) and was nearly as high in the spleen 2 d after treatment with CDN/H9-MSA (*SI Appendix*, Fig. S10 *C* and *D*). It is highly unlikely that such a high percentage of all NK cells trafficked through the site of treatment in this short period.

Mechanistically, the synergistic antitumor effects of CDN and H9-MSA were manifested primarily by greater induction of NK cell activation, cytotoxicity, and granzyme B expression, as well as some impact on NK cell proliferation. Type I IFNs induced by i.t. injections of CDN act directly on NK cells to induce granzymes and cytotoxicity (32, 44) and protection from fratricide (45) and indirectly by inducing IL-15Rα/IL-15 complexes on DCs, which are *trans*-presented to NK cells (32, 46). The early bursts of IFN and IL-15 induced by administration of CDN are not sustained, however, consistent with the rapid waning of NK activity we observed with CDN alone. NK cells that infiltrate MHC I–deficient tumors are also prone to enter a state of hyporesponsiveness or anergy, which can be delayed or reversed with injections of cytokines, including H9, or a mixture of IL-12 and IL-18 (47). Together, these mechanisms are likely to account for the synergistic effects of combining H9-MSA and CDN therapy.

Compared with high-dose IL-2, the H9 superkine was previously shown to provide greater antitumor efficacy yet lower toxicity with lower accumulation of Tregs (35). Published studies show greater efficacy of IL-2 and other cytokines with half life–extending modifications, such as fusion to albumin or Fc domains, or PEGylation (37, 48). We observed that extended–half life H9 was more effective than extended–half life IL-2 in the context of combination therapy as well. We observed acceptable toxicity in mice receiving the combination therapy, generally maintaining a normal body score, but acknowledge further assessment of toxicity is needed. Considering these results, H9-MSA warrants consideration for clinical applications. Combining CDN therapy with other half life–extended IL-2 and IL-15 variants, several of which are undergoing clinical testing (48), may also be effective.
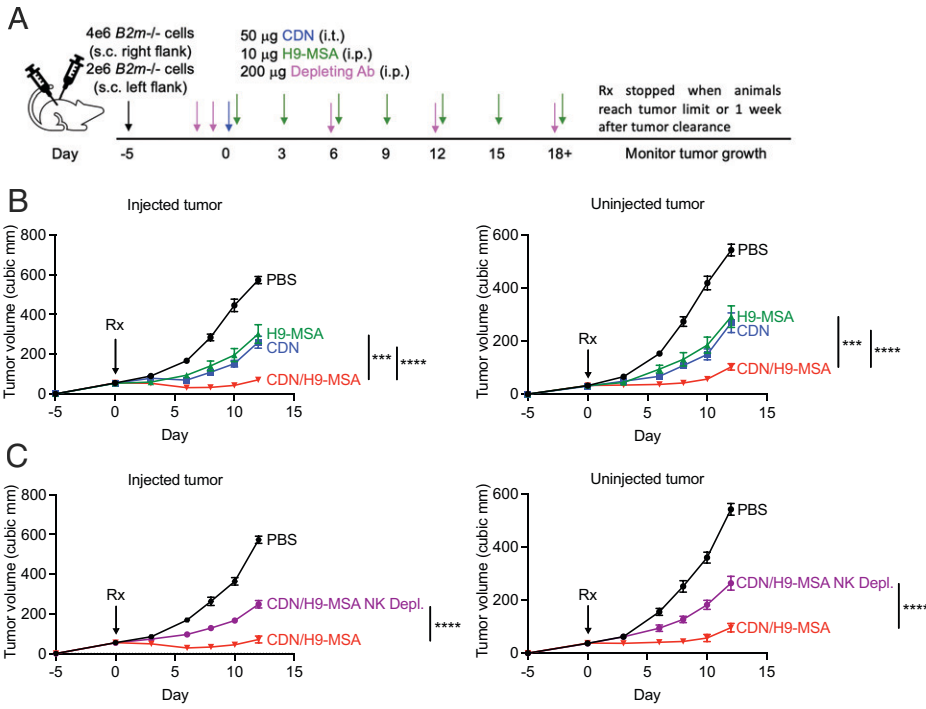
Fig. 5. Intratumoral CDN injections combined with i.p. H9-MSA injections synergized in creating a systemic NK cell–mediated antitumor effect. (*A*) Timeline of the bilateral tumor experiments. On day −5, B16-F10-*B2m*$^{-/-}$ tumor cells were injected s.c. into both flanks of C57BL/6J mice. Mice were depleted of CD4 cells and CD8 cells 2 and 1 d before initiation of treatment. On day 0, the right-flank tumor was injected once i.t. with 50 μg of CDN or PBS. The mice received i.p. injections of PBS or 10 μg of H9-MSA starting on day 0 and again every 3 d until mice were killed. (*B*) Growth of injected (*Left*) vs. contra-lateral uninjected tumors (*Right*) receiving the indicated therapies. The data were combined from three experiments (*n* = 18). (*C*) Tumor growth following CDN/H9-MSA therapy in mice from which NK cells were depleted or not (with the treatment schedule shown in *A* as indicated). The data were combined from two experiments (*n* = 12). Tumor growth data were analyzed by two-way ANOVA. Error bars represent standard error of the mean (SEM). ***$P < 0.001$, ****$P < 0.0001$.

In syngeneic tumor transplant models, H9-MSA acted synergistically not only with CDN but also with another agonist for the innate immune system, CpG ODN DS-L03, a TLR9 agonist optimized to stimulate high levels of type I IFN (49). These findings show the promise of combining IL-2/IL-15 family cytokines with agents that induce IRF3 and NF-κB signaling. Clinical trials of TLR agonists and STING agonists as cancer therapies have thus far yielded mixed results but clinical development remains active (33, 34, 50). Many engineered forms of IL-2 family cytokines, including PEGylated IL-2, Fc-bound, and engineered partial agonists, are currently being investigated in many clinical and preclinical trials (48). Our findings suggest that those variants should be tested in combination with innate agonists such as STING agonists to improve overall outcomes. The greater challenges of treating human cancer versus mouse cancer models are well-documented and may reflect later diagnosis, a relatively older population in the case of human patients, and the frequent use of transplantable mouse cancer models as opposed to primary cancer models, among other factors. Our results with primary sarcomas were encouraging, however, and suggest that the synergistic effects of combining innate agonists and IL-2 family cytokines may have considerable promise in clinical applications.

The therapeutic effects of CDN/H9-MSA combination therapy were mediated by different effector cells depending on the tumor cell line studied and whether the tumor cells expressed MHC I molecules. In two difficult-to-treat MHC I–deficient tumor models, NK cells were critical for tumor rejection after combination therapy. Remarkably, in the MC38-*B2m*$^{-/-}$ model, the treatment effectively cured 100% of tumor-bearing *Rag2*$^{-/-}$ mice, which lack T cells. NK cells were essential for these dramatic effects. In the B16-F10-*B2m*$^{-/-}$ model, NK cells and CD4 T cells each caused weaker tumor rejection separately, but together resulted in long-term survival in the large majority of the animals. The less effective NK cell responses in the B16-F10-*B2m*$^{-/-}$ model could be related to the absence of NKG2D ligands, which are present on MC38 cells but not B16 cells (19).

The mechanism of tumor elimination by CD4$^+$ T cells is unknown. It could be due to cytokine action, mobilization of effector myeloid cells, or direct recognition by the CD4$^+$ T cells of MHC II on tumor cells and subsequent tumor cell killing (39, 51, 52). The elicitation of antitumor CD4 T cells in the B16-F10-*B2m*$^{-/-}$ model, but not the MC38-*B2m*$^{-/-}$ model, might be explained by the finding that MHC II expression can be induced on B16-F10 cells in vivo (39). However, other distinctive features of the tumor cells may also be at play, given that antitumor CD4 T cells have been described for B16 tumor cells in several other scenarios (39, 51, 52).

In the context of MHC I$^+$ B16-F10 tumors, a "cold" tumor model that is resistant to checkpoint therapy and other experimental monotherapies (53), CDN/H9-MSA therapy induced a highly effective CD8 T cell–mediated antitumor response, with no evidence for roles of NK cells or CD4 T cells. The impressive impact of CDN/H9-MSA therapy shown here is notable considering that durable antitumor responses in this model have required combining three or four agents in past studies (31, 54). The absence of effective antitumor NK cells in this model with CDN/H9-MSA therapy can be explained by the inhibitory effects of MHC I, but it remains unclear why effective antitumor CD4 T cells were not elicited.

In the absence of T cells and NK cells, the combination therapy still delayed tumor growth in all the tumor models studied but did not result in long-term remissions. Our data suggest that therapy-induced production of TNF-α, which alters the tumor vasculature, and type I IFNs, which inhibit cell proliferation, are partly responsible for the residual antitumor effects and are supported by the observation of increased serum IFN after a single i.t. CDN injection (32). It remains possible that the therapy combination also induces other antitumor cytokines or other cell types that retard tumor growth, such as myeloid cells or other innate lymphoid cell subtypes.

The finding that CDN/H9-MSA therapy worked well for both MHC I$^+$ cold tumors and MHC I–deficient tumor variants suggests the promise of this approach both for tumor types that are resistant to checkpoint therapy and for preventing the emergence of MHC I–deficient tumor variants during
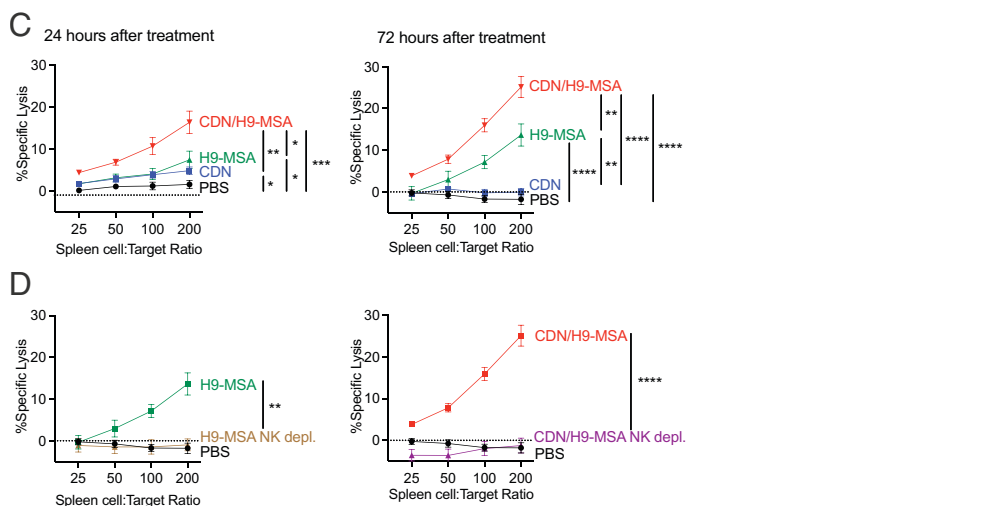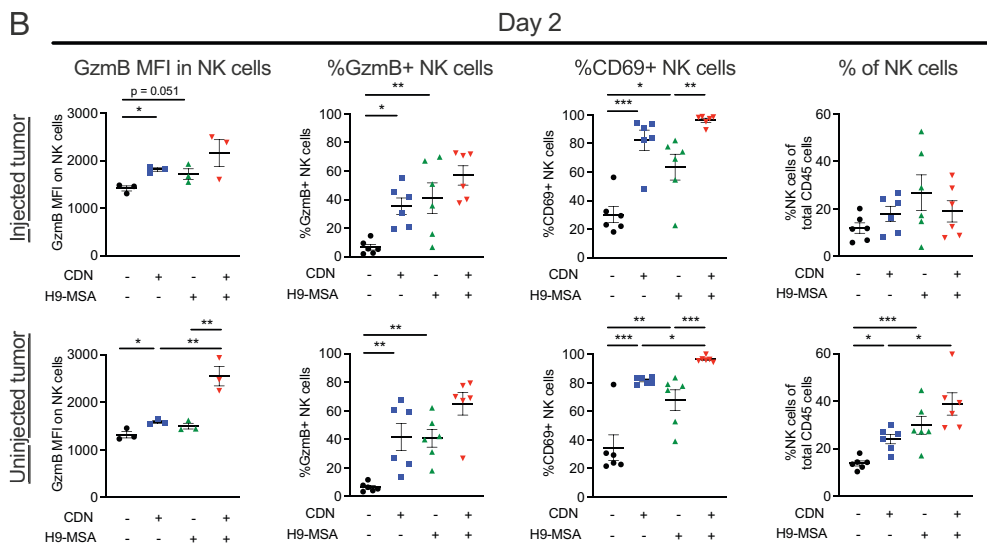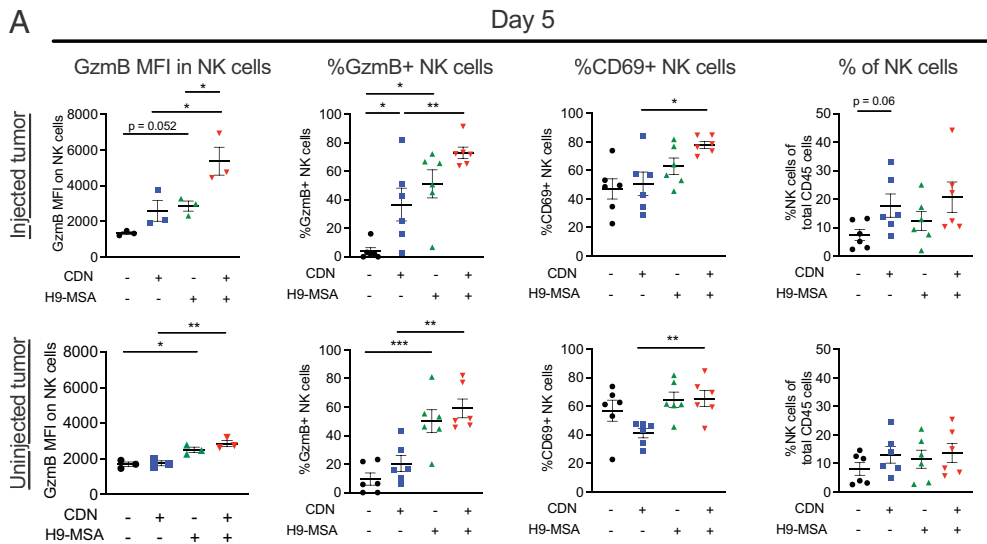
Fig. 6. Activation, proliferation, and cytotoxicity of NK cells in tumor-bearing mice receiving CDN/H9-MSA immunotherapy. B16-F10-$B2m^{-/-}$ tumors were established on both flanks of C57BL/6J mice as in Fig. 5. (A and B) On day 5 (A) or day 2 (B), single-cell suspensions of both tumors were examined for the intracellular or cell-surface markers shown and the percentages of NK cells among viable CD45$^+$ cells. $n = 3$. GzmB mean fluorescence intensity (MFI) data are representative of at least two independent experiments ($n = 3$) and all other data were combined from two independent experiments ($n = 6$). Samples were analyzed by one-way ANOVA. (C) B16-F10-$B2m^{-/-}$ tumors were established and treated as described in Fig. 5. Twenty-four and 72 h after treatment, splenocytes were tested for cytotoxicity of B16-F10-$B2m^{-/-}$ target cells. Spontaneous lysis of these target cells averaged 11%. Error bars are shown for biological replicates ($n = 8$). (D) B16-F10-$B2m^{-/-}$ tumors were established, treated, and tested as in C, 72 h after initiating H9-MSA therapy or combination therapy, as indicated. Additionally, mice in one group receiving each therapy were depleted of NK cells. $n = 8$ biological replicates. Data in C and D were combined from two independent experiments and were analyzed by two-way ANOVA. Error bars represent standard error of the mean (SEM). $n = 8$. *$P < 0.05$, **$P < 0.01$, ***$P < 0.001$, ****$P < 0.0001$.

immunotherapy. The loss of MHC I expression may occur before or during immunotherapy and is increasingly recognized as a significant mechanism of acquired resistance of tumors to checkpoint therapy (8–10, 55, 56).

CDN and H9-MSA also synergized in the MCA sarcoma model, leading to highly delayed tumor growth and extended survival. Both NK cells and T cells contributed to the therapeutic

effect, providing a demonstration that this therapy combination can mobilize both types of responses in the same tumor model. The addition of checkpoint therapy to the CDN/H9-MSA therapy regimen resulted in tumor regressions and long-term tumor-free survival in ~44% of the treated animals. These findings represent a dramatic example of long-term immunotherapy remissions in an autochthonous sarcoma model in mice, which is
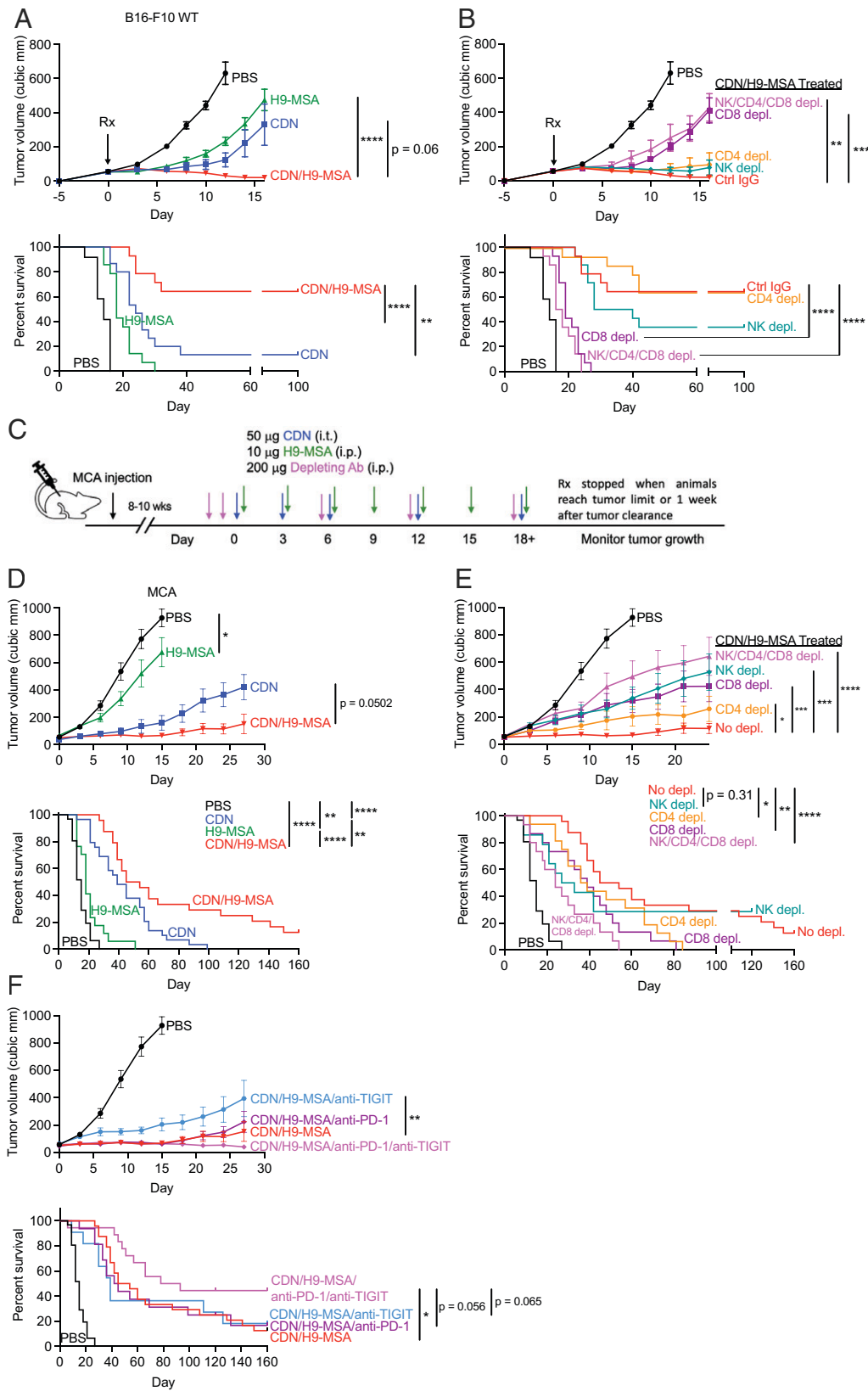
Fig. 7. CDN/H9-MSA therapy induced potent antitumor effects with MHC I⁺ tumors, mediated by CD8 T cells. (*A* and *B*) Experiments were carried out as in Fig. 1 except MHC I⁺ B16-F10 WT cells were employed. (*A*) Impact of CDN, H9-MSA, or combination therapy. (*B*) Antitumor effects were reversed by depleting CD8 T cells ($P < 0.0001$), with no significant impacts of depleting NK cells or CD4 T cells (P, not significant). Tumor growth data were analyzed by two-way ANOVA. Survival data were analyzed using log-rank (Mantel–Cox) tests. The data are representative of two independent experiments. $n = 6$ or 7 mice per group. (*C*) Timeline for MCA-induced tumors. When MCA-induced tumors reached ~50 mm³ in size, they were injected i.t. with PBS or 50 μg of CDN on days 0, 3, and 6 and repeated every 6 d thereafter. Mice were also injected i.p. with PBS or 10 μg of H9-MSA starting on day 0, which was repeated every 3 d. In some groups, mice were depleted of NK cells, CD8 T cells, or CD4 T cells, or injected with control IgG. (*D*) Tumor growth curves and survival of mice. (*E*) Tumor growth curves and survival of depleted mice. (*F*) Addition of checkpoint inhibitors consisting of i.p. injections of anti–PD-1 (clone RMP1-14) and anti-TIGIT (clone MUR10A) increased tumor rejection and overall survival. Data are a combination of multiple experiments, such that some of the data (e.g., CDN/H9-MSA) are shared in different panels. Data were analyzed by two-way ANOVA. $n = 11$ to 24. Error bars represent standard error of the mean (SEM). *$P < 0.05$, **$P < 0.01$, ***$P < 0.001$, ****$P < 0.0001$.

an especially substantive outcome considering that immunotherapy has given generally poor outcomes in treating human sarcomas (57). Given that the schedule of treatments had an impact on toxicity of the therapy, any consideration of using such a regimen in human patients would require careful tests of different schedules of the individual therapeutics.

In conclusion, our results show that CDN therapy combined with the IL-2 superkine, H9-MSA, effectively enhanced the rejection of MHC I⁺ and MHC I–deficient tumors, as well as primary carcinogen-induced sarcomas. The CDN/H9-MSA treatments proved to be remarkably effective against difficult-to-treat tumors, mobilizing various effector cells depending on

tumor cell type and MHC I expression. These results provide compelling support for testing combinations of innate immune system agonists and IL-2 family superkines as potential next-generation immunotherapies for tumors that are resistant to currently approved immunotherapy regimens.

Materials and Methods

Study Design. For most experiments in this study, tumors were established s.c. in mice, PBS or CDN was injected i.t. once, and PBS or H9-MSA was injected i.p. multiple times. Tumor growth, toxicity, overall survival, and NK cell activation status were recorded. Male and female mice were used equally within an experiment, and treatments were randomized among mice in the same cage. Experimental groups consisted of 5 to 10 mice. Mice were terminated in the studies when tumors reached an average diameter of 1.5 cm or mice showed a body condition score of less than 2. We did not use a power analysis to calculate sample size. All experiments were performed at least twice and, in some cases, experiments were pooled. The investigators were not blinded.

Mouse Strains. Mice were maintained at the University of California (UC), Berkeley. C57BL/6J and $Rag2^{-/-}$ mice were purchased from the Jackson Laboratory. All mice used were between 8 and 20 wk of age. All experiments were approved by the UC Berkeley Animal Care and Use Committee and were performed in adherence to the NIH *Guide for the Care and Use of Laboratory Animals* (58).

Cell Lines and Culture Conditions. B16-F10 cells, obtained from the UC Berkeley Cell Culture Facility, and MC38 cells, obtained from J. P. Allison (M.D. Anderson Cancer Center, Houston, TX), were cultured in Dulbecco's modified Eagle's medium (Thermo Fisher Scientific). $B2m^{-/-}$ versions of both B16-F10 and MC38 were previously generated in the laboratory using CRISPR-Cas9 (32). In all cases, medium contained 5% fetal bovine serum (FBS) (Omega Scientific), 0.2 mg/mL glutamine (Sigma-Aldrich), 100 U/mL penicillin (Thermo Fisher Scientific), 100 µg/mL streptomycin (Thermo Fisher Scientific), 10 µg/mL gentamicin sulfate (Thermo Fisher Scientific), 50 µM β-mercaptoethanol (EMD Biosciences), and 20 mM Hepes (Thermo Fisher Scientific). Cells were cultured in 5% CO_2. All cell lines tested negative for mycoplasma contamination.

Protein Design and Purification. DNA encoding WT human IL-2 or human IL-2 with H9 mutations (L80F, R81D, L85V, I86V, I92F) (34) was cloned into the insect expression vector pAcGP67-A, which includes a C-terminal 8×HIS tag for affinity purification. DNA encoding MSA was purchased from Integrated DNA Technologies and cloned into pAcGP67-A as an N-terminal fusion between the N terminus of human IL-2 and C terminus of MSA (indicated as IL-2-MSA or H9-MSA).

Insect expression DNA constructs were transfected into *Trichoplusia ni* (High Five) cells (Invitrogen) using the BaculoGold Baculovirus Expression System (BD Biosciences) for secretion, purified from the clarified supernatant via Ni-NTA followed by size-exclusion chromatography with a Superdex-200 column, and formulated in sterile PBS (Gibco). Endotoxin was removed using the Proteus NoEndo HC Spin Column Kit following the manufacturer's recommendations (Vivaproducts) and removal (to a final amount of between 0.01-1.1 EU/mg of protein) was confirmed using the Pierce LAL Chromogenic Endotoxin Quantitation Kit (Thermo Fisher Scientific). IL-2 proteins were concentrated and stored at −80 °C until use.

In Vivo Tumor Transplant Experiments. Cells were washed and resuspended in PBS (Thermo Fisher Scientific), and 100 µL containing 4×10^6 cells was injected subcutaneously. Tumor volume was estimated using the ellipsoid formula: $V = (4/3)\pi abc$, where a, b, and c correspond to height, width, and length, respectively, of the tumors measured with digital calipers. Five days after tumor cell inoculation, when tumors reached a volume of 50 mm^3, they were injected i.t. with PBS or 50 µg of the STING agonist mixed-linkage [2′,3′] dithio-(Rp,Rp) cyclic diadenosine monophosphate (ADU-S100, abbreviated as CDN in this paper) in a total volume of 100 µL PBS. Mice were also injected i.p. with PBS, 20 µg of H9, 10 µg of IL-2-MSA, or 10 µg of H9-MSA in a total volume of 100 µL PBS, which was repeated every 3 d (except for *SI Appendix*, Fig. S1, where it was repeated every 2 d) until the mice were killed or 1 wk after a mouse had no palpable tumor. For the comparison of innate simulants, mice were injected i.t. with PBS or 50 µg of either CDN or CpG ODN DS-L03 (Invivogen) in a total volume of 100 µL PBS.

Bilateral Tumor Experiments. All mice were depleted of CD4 and CD8 T cells. Tumor cells were washed and resuspended in PBS; 100 µL containing 4×10^6 cells was injected s.c. into the right flank of the mice and 100 µL containing 2×10^6 cells was injected s.c. into the left flank of the mice. Tumor growth was measured using digital calipers and tumor volume was estimated using the ellipsoid formula: $V = (4/3)\pi abc$. Five days after tumor inoculation, when the right-flank tumors were ~50 to 100 mm^3, the right-flank tumors were injected i.t. with PBS or CDN and the mice were treated i.p. with H9-MSA or PBS as described above for single-tumor experiments.

MCA-Induced Sarcoma Experiments. Mice were injected s.c. into the right flank with 100 µg of 3-methylcholanthrene (MCA) (Crescent Chemical) in peanut oil, after which they were monitored weekly. When palpable tumors (~50 mm^3) were detected, usually 8 to 10 wk after MCA injection, the mice were randomized and entered into the study. Tumors were injected i.t. with PBS or 50 µg of CDN in a total volume of 100 µL PBS on days 0, 3, and 6, which was repeated every 6 d. Mice were also injected i.p. with PBS or 10 µg of H9-MSA in a total volume of 100 µL PBS starting on day 0, which was repeated every 3 d.

In Vivo Cellular Depletions, Checkpoint Therapy, and Cytokine Blockade Experiments. In some experiments, mice were depleted of NK cells, CD8 cells, and/or CD4 cells by i.p. injections of 200 µg of anti-NK1.1 (clone PK136, purified in our laboratory), anti-CD8β.2 (clone 53-5.8, Leinco), or anti-CD4 (clone GK1.5, Leinco), respectively, 2 and 1 d before initiation of therapy, and again every 6 d thereafter until mice were killed or no palpable tumor was detected for 1 wk. Whole rat immunoglobulin G (IgG; Jackson ImmunoResearch) was used as a control for depletions. Depletions were confirmed by flow cytometry. In some experiments, mice received 500 µg of anti–IFNAR-1 (clone MAR1-5A3, Leinco) or 200 µg of anti–TNF-α (clone TN3-19.12, Leinco) i.p. on days −1 and 0 before the initiation of therapy, and again every 3 d throughout the experiment.

In some MCA experiments, mice received additional therapy, in the form of 200 µg of anti-PD-1 (clone RMP1-14, Leinco) and/or 200 µg of anti-TIGIT (clone MUR10A from Arcus Biosciences or 1G9 from BioXCell), each in a volume of 100 µL PBS, every 3 d. In most cases, the anti-TIGIT was staggered 1 d after anti–PD-1 treatment, but in some cases it was injected on the same day.

Toxicity. To assess toxicity of the CDN/H9-MSA treatment, tumors were established and mice were treated i.t. with PBS or 50 µg of CDN and i.p. with PBS or 10 or 20 µg of H9-MSA. Mouse weights were recorded daily. Pulmonary edema was determined by measurement of lung wet weight/body weight ratios 6 d after initiating treatment.

Flow Cytometry. Single-cell suspensions of tumors were generated by dicing tumors with a razor blade followed by enzymatic digestion for 30 min at 37 °C in medium containing 1 mg/mL collagenase D (Roche Diagnostics) and 1 µg/mL DNase I (Thermo Fisher Scientific). The samples were further dissociated in a gentleMACS dissociator (Miltenyi) before passage through a 70-µm filter. Cells were stained directly for determining NK cell numbers and Ki67 staining or incubated for 4 h in medium containing brefeldin A (BioLegend) and monensin (BioLegend) for granzyme B staining before surface staining and intracellular staining. LIVE/DEAD stain (Thermo Fisher Scientific) was used to exclude dead cells. Before staining with antibodies, FcgRII/III receptors were blocked by resuspending the cells in undiluted culture supernatant of the 2.4G2 hybridoma cell line (prepared in the laboratory) and incubating for 20 min at 4 °C. Cells were washed in PBS containing 2.5% fetal calf serum and stained with antibodies directly conjugated to fluorochromes for 30 min at 4 °C in the same buffer. For intracellular staining of granzyme B and Ki67, cells were fixed and permeabilized using Cytofix/Cytoperm buffer (BD Biosciences) and stained with antibodies directly conjugated to fluorochromes for 1 h at room temperature in 1× Perm/Wash buffer (BD Biosciences). NK cells were gated as viable, CD45$^+$, CD3$^-$, CD19$^-$, F4/80$^-$, Ter119$^-$, NK1.1$^+$, NKp46$^+$ cells. Flow cytometry was performed using an LSRFortessa or an LSRFortessa X-20 (BD Biosciences). Data were analyzed using FlowJo software.

Antibodies for Flow Cytometry. The following antibodies were used (all purchased from BioLegend): anti-CD45 (30-F11, Alexa Fluor 700), anti-CD3ε (145-2C11, APC-Cy7, PE-Cy5), anti-CD4 (GK1.5, BV421), anti-CD8a (53-6.7, BV650), anti-CD19 (6D5, PE-Cy5), anti-Ter119 (TER-119, PE-Cy5), anti-F4/80 (BM8, PE-Cy5), anti-NKp46 (29A1.4, PerCP-Cy5.5), anti-NK1.1 (PK136, BV711, FITC), anti-

CD69 (H1.2F3, BV605), anti-Sca1 (D7, BV510), anti-Ki67 (SolA15, eFluor 450), anti-CD107a (1D4B, Alexa Fluor 647), and anti-IFNγ (XMG1.2, PE). Anti–granzyme B (GB11, PE-CF594) was purchased from BD Biosciences.

Ex Vivo Cytotoxicity Assay. Cytotoxicity by splenocytes was assessed with a standard 5-h ^{51}Cr-release assay. Twenty-four and 72 h after treating mice with PBS, CDN (i.t.), H9-MSA (i.p.), or CDN/H9-MSA, spleens were harvested and single-cell suspensions were treated with ACK lysis buffer. The ^{51}Cr-release assay was performed as described [Nicolai et al., 2020, (32)] using B16-F10-$B2m^{-/-}$ cells as target cells. For NK cell–depleted samples, mice were injected twice (2 and 1 d before the initiation of treatment) i.p. with 200 μg of anti-NK1.1 (PK136) and spleens were collected and treated as described above. Efficacies of cellular depletions were confirmed by flow cytometry.

Statistics. Statistics were performed using Prism (GraphPad). For tumor growth and survival data, two-way ANOVA and log-rank (Mantel–Cox) tests were used. Two-way ANOVA was used for cytotoxicity. For flow cytometry data, single therapies were compared with either control PBS or CDN/H9-MSA using one-way ANOVA followed by Dunnett's multiple comparisons. Significance is indicated as follows: *$P < 0.05$, **$P < 0.01$, ***$P < 0.001$, ****$P < 0.0001$.

Data Availability. The CDN used in this study was provided under a material transfer agreement from Aduro Biotech (now Chinook Therapeutics), but molecularly identical CDN can be purchased. The H9 sequence is published (35) and is available to any investigator who would like to generate the protein.

All study data are included in the article and/or *SI Appendix*.

Author affiliations: ᵃDivision of Immunology and Molecular Medicine, Department of Molecular and Cell Biology, University of California, Berkeley, CA 94720; ᵇHHMI, Stanford University School of Medicine, Stanford, CA 94305; ᶜDepartment of Molecular and Cellular Physiology, Stanford University School of Medicine, Stanford, CA 94305; ᵈDepartment of Structural Biology, Stanford University School of Medicine, Stanford, CA 94305; and ᵉAduro Biotech, Inc., Berkeley, CA 94710

1. P. Sharma et al., The next decade of immune checkpoint therapy. Cancer Discov. 11, 838–857 (2021).
2. A. Kalbasi, A. Ribas, Tumour-intrinsic resistance to immune checkpoint blockade. Nat. Rev. Immunol. 20, 25–39 (2020).
3. D. R. Leach, M. F. Krummel, J. P. Allison, Enhancement of antitumor immunity by CTLA-4 blockade. Science 271, 1734–1736 (1996).
4. L. B. Alexandrov et al.; Australian Pancreatic Cancer Genome Initiative; ICGC Breast Cancer Consortium; ICGC MMML-Seq Consortium; ICGC PedBrain, Signatures of mutational processes in human cancer. Nature 500, 415–421 (2013).
5. M. Yarchoan, A. Hopkins, E. M. Jaffee, Tumor mutational burden and response rate to PD-1 inhibition. N. Engl. J. Med. 377, 2500–2501 (2017).
6. F. Garrido, I. Algarra, MHC antigens and tumor escape from immune surveillance. Adv. Cancer Res. 83, 117–158 (2001).
7. M. G. Roemer et al., Classical Hodgkin lymphoma with reduced β2M/MHC class I expression is associated with inferior outcome independent of 9p24.1 status. Cancer Immunol. Res. 4, 910–916 (2016).
8. N. McGranahan et al.; TRACERx Consortium, Allele-specific HLA loss and immune escape in lung cancer evolution. Cell 171, 1259–1271 (2017).
9. I. Maleno et al., Frequent loss of heterozygosity in the β2-microglobulin region of chromosome 15 in primary human tumors. Immunogenetics 63, 65–71 (2011).
10. M. Sade-Feldman et al., Resistance to checkpoint blockade therapy through inactivation of antigen presentation. Nat. Commun. 8, 1136 (2017).
11. A. Marcus et al., Recognition of tumors by the innate immune system and natural killer cells. Adv. Immunol. 122, 91–128 (2014).
12. E. Vivier et al., Innate or adaptive immunity? The example of natural killer cells. Science 331, 44–49 (2011).
13. S. Bauer et al., Activation of NK cells and T cells by NKG2D, a receptor for stress-inducible MICA. Science 285, 727–729 (1999).
14. D. H. Raulet, N. Guerra, Oncogenic stress sensed by the immune system: Role of natural killer cell receptors. Nat. Rev. Immunol. 9, 568–580 (2009).
15. K. C. Barry et al., A natural killer-dendritic cell axis defines checkpoint therapy-responsive tumor microenvironments. Nat. Med. 24, 1178–1191 (2018).
16. C. J. Kearney et al., Tumor immune evasion arises through loss of TNF sensitivity. Sci. Immunol. 3, eaar3451 (2018).
17. J. P. Böttcher et al., NK cells stimulate recruitment of cDC1 into the tumor microenvironment promoting cancer immune control. Cell 172, 1022–1037.e14 (2018).
18. D. H. Raulet, S. Gasser, B. G. Gowen, W. Deng, H. Jung, Regulation of ligands for the NKG2D activating receptor. Annu. Rev. Immunol. 31, 413–441 (2013).
19. A. M. Jamieson et al., The role of the NKG2D immunoreceptor in immune cell activation and natural killing. Immunity 17, 19–29 (2002).
20. F. M. Karlhofer, R. K. Ribaudo, W. M. Yokoyama, MHC class I alloantigen specificity of Ly-49⁺ IL-2-activated natural killer cells. Nature 358, 66–70 (1992).
21. A. Moretta, L. Moretta, HLA class I specific inhibitory receptors. Curr. Opin. Immunol. 9, 694–701 (1997).
22. N. Shifrin, D. H. Raulet, M. Ardolino, NK cell self tolerance, responsiveness and missing self recognition. Semin. Immunol. 26, 138–144 (2014).
23. L. Sun, J. Wu, F. Du, X. Chen, Z. J. Chen, Cyclic GMP-AMP synthase is a cytosolic DNA sensor that activates the type I interferon pathway. Science 339, 786–791 (2013).
24. E. J. Diner et al., The innate immune DNA sensor cGAS produces a noncanonical cyclic dinucleotide that activates human STING. Cell Rep. 3, 1355–1361 (2013).
25. J. Wu et al., Cyclic GMP-AMP is an endogenous second messenger in innate immune signaling by cytosolic DNA. Science 339, 826–830 (2013).
26. D. Gao et al., Cyclic GMP-AMP synthase is an innate immune sensor of HIV and other retroviruses. Science 341, 903–906 (2013).
27. H. Ishikawa, G. N. Barber, STING is an endoplasmic reticulum adaptor that facilitates innate immune signalling. Nature 455, 674–678 (2008).
28. A. Marcus et al., Tumor-derived cGAMP triggers a STING-mediated interferon response in non-tumor cells to activate the NK cell response. Immunity 49, 754–763.e4 (2018).
29. S. R. Woo et al., STING-dependent cytosolic DNA sensing mediates innate immune recognition of immunogenic tumors. Immunity 41, 830–842 (2014).
30. L. Corrales et al., Direct activation of STING in the tumor microenvironment leads to potent and systemic tumor regression and immunity. Cell Rep. 11, 1018–1030 (2015).
31. K. E. Sivick et al., Magnitude of therapeutic STING activation determines CD8⁺ T cell-mediated anti-tumor immunity. Cell Rep. 25, 3074–3085.e5 (2018).
32. C. J. Nicolai et al., NK cells mediate clearance of CD8⁺ T cell-resistant tumors in response to STING agonists. Sci. Immunol. 5, eaaz2738 (2020).
33. K. J. Harrington et al., Preliminary results of the first-in-human (FIH) study of MK-1454, an agonist of stimulator of interferon genes (STING), as monotherapy or in combination with pembrolizumab (pembro) in patients with advanced solid tumors or lymphomas. Ann. Oncol. 29 (suppl. 8), VIII712 (2018).
34. F. Meric-Bernstam et al., Phase Ib study of MIW815 (ADU-S100) in combination with spartalizumab (PDR001) in patients (pts) with advanced/metastatic solid tumors or lymphomas. J. Clin. Oncol. 37, 2507 (2019).
35. A. M. Levin et al., Exploiting a natural conformational switch to engineer an interleukin-2 'superkine.' Nature 484, 529–533 (2012).
36. M. Ardolino, D. H. Raulet, Cytokine therapy restores antitumor responses of NK cells rendered anergic in MHC I-deficient tumors. OncoImmunology 5, e1002725 (2015).
37. E. F. Zhu et al., Synergistic innate and adaptive immune response to combination immunotherapy with anti-tumor antigen antibodies and extended serum half-life IL-2. Cancer Cell 27, 489–501 (2015).
38. E. F. Conant, K. R. Fox, W. T. Miller, Pulmonary edema as a complication of interleukin-2 therapy. AJR Am. J. Roentgenol. 152, 749–752 (1989).
39. S. A. Quezada et al., Tumor-reactive CD4⁺ T cells develop cytotoxic activity and eradicate large established melanoma after transfer into lymphopenic hosts. J. Exp. Med. 207, 637–650 (2010).
40. R. E. Tay, E. K. Richardson, H. C. Toh, Revisiting the role of CD4⁺ T cells in cancer immunotherapy–New insights into old paradigms. Cancer Gene Ther. 28, 5–17 (2021).
41. B. J. Francica et al., TNFα and radioresistant stromal cells are essential for therapeutic efficacy of cyclic dinucleotide STING agonists in nonimmunogenic tumors. Cancer Immunol. Res. 6, 422–433 (2018).
42. P. Sharma, J. P. Allison, Immune checkpoint targeting in cancer therapy: Toward combination strategies with curative potential. Cell 161, 205–214 (2015).
43. A. Ribas, J. D. Wolchok, Cancer immunotherapy using checkpoint blockade. Science 359, 1350–1355 (2018).
44. J. Martinez, X. Huang, Y. Yang, Direct action of type I IFN on NK cells is required for their activation in response to vaccinia viral infection in vivo. J. Immunol. 180, 1592–1597 (2008).
45. S. Madera et al., Type I IFN promotes NK cell expansion during viral infection by protecting NK cells against fratricide. J. Exp. Med. 213, 225–233 (2016).
46. M. Lucas, W. Schachterle, K. Oberle, P. Aichele, A. Diefenbach, Dendritic cells prime natural killer cells by trans-presenting interleukin 15. Immunity 26, 503–517 (2007).

47. M. Ardolino et al., Cytokine therapy reverses NK cell anergy in MHC-deficient tumors. *J. Clin. Invest.* **124**, 4781–4794 (2014).

48. A. Mullard, Restoring IL-2 to its cancer immunotherapy glory. *Nat. Rev. Drug Discov.* **20**, 163–165 (2021).

49. L. Yang et al., CpG oligodeoxynucleotides with double stem-loops show strong immunostimulatory activity. *Int. Immunopharmacol.* **15**, 89–96 (2013).

50. S. M. McWhirter, C. A. Jefferies, Nucleic acid sensors as therapeutic targets for human disease. *Immunity* **53**, 78–97 (2020).

51. O. A. Haabeth et al., How do CD4(+) T cells detect and eliminate tumor cells that either lack or express MHC class II molecules? *Front. Immunol.* **5**, 174 (2014).

52. Y. Xie et al., Naive tumor-specific CD4(+) T cells differentiated in vivo eradicate established melanoma. *J. Exp. Med.* **207**, 651–667 (2010).

53. M. G. Lechner et al., Immunogenicity of murine solid tumor models as a defining feature of in vivo behavior and response to immunotherapy. *J. Immunother.* **36**, 477–489 (2013).

54. K. D. Moynihan et al., Eradication of large established tumors in mice by combination immunotherapy that engages innate and adaptive immune responses. *Nat. Med.* **22**, 1402–1410 (2016).

55. J. M. Zaretsky et al., Mutations associated with acquired resistance to PD-1 blockade in melanoma. *N. Engl. J. Med.* **375**, 819–829 (2016).

56. F. Garrido, N. Aptsiauri, E. M. Doorduijn, A. M. Garcia Lora, T. van Hall, The urgent need to recover MHC class I in cancers for effective immunotherapy. *Curr. Opin. Immunol.* **39**, 44–51 (2016).

57. H. K. Birdi et al., Immunotherapy for sarcomas: New frontiers and unveiled opportunities. *J. Immunother. Cancer* **9**, e001580 (2021).

58. National Research Council, *Guide for the Care and Use of Laboratory Animals* (National Academies Press, Washington, DC, ed. 8, 2011).

Supporting Information
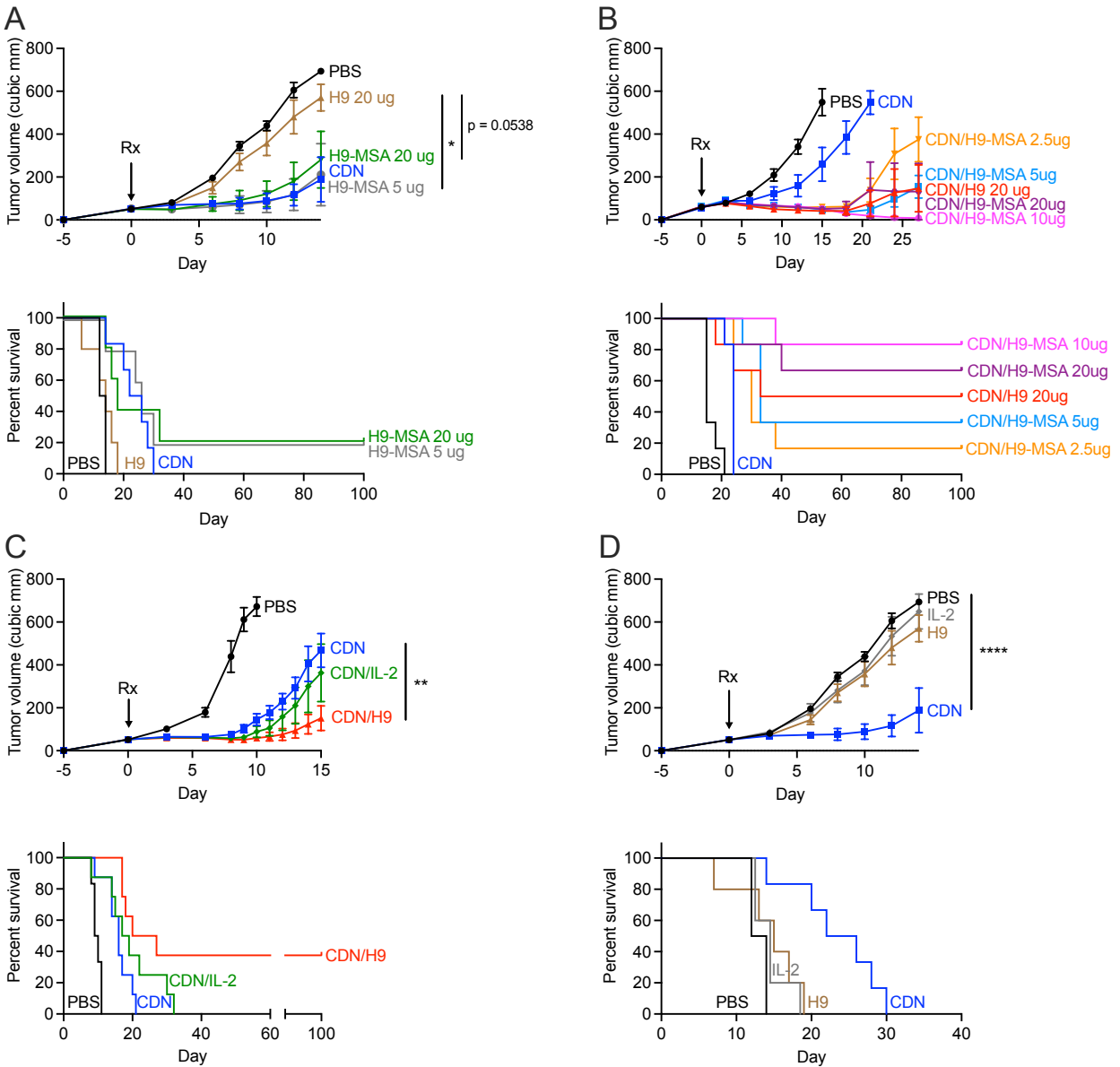
Figure S1. Synergistic impact of H9 or H9-MSA administration and CDN therapy on tumor rejection. B16-F10 *B2m-/-* tumor cells were implanted s.c.in C57BL/6J mice on day -5 and grown to approximately 50 mm³. On d0, tumors were injected once intratumorally with 50 μg CDN or PBS, and/or i.p. with the indicated cytokines or PBS. Cytokine administrations were repeated every two days until mice were euthanized or until 1 week after a mouse completely

1

cleared a tumor. Tumor growth curves and survival data are shown. **(A)** Half-life extended H9

(H9-MSA) showed significant antitumor effects as a monotherapy, even with a lower

administered dose (5 µg). **(B)** Dose titration of H9-MSA in combination with CDN therapy,

showing that doses >5 µg were necessary for optimal combination therapy effects. **(C)** When

combined with CDN therapy, H9 administration, but not IL-2 administration, resulted in

improved antitumor effects including long term survival of a significant percentage of the

animals. **(D)** CDN monotherapy, but not monotherapy with IL-2 or H9, delayed tumor growth.

The data in panels A-C were from one large experiment. Tumor growth data were analyzed by 2-

way ANOVA. Survival data were analyzed using log-rank (Mantel-Cox) tests. The data in all

panels are representative of two independent experiments. n=6-7 mice per group.
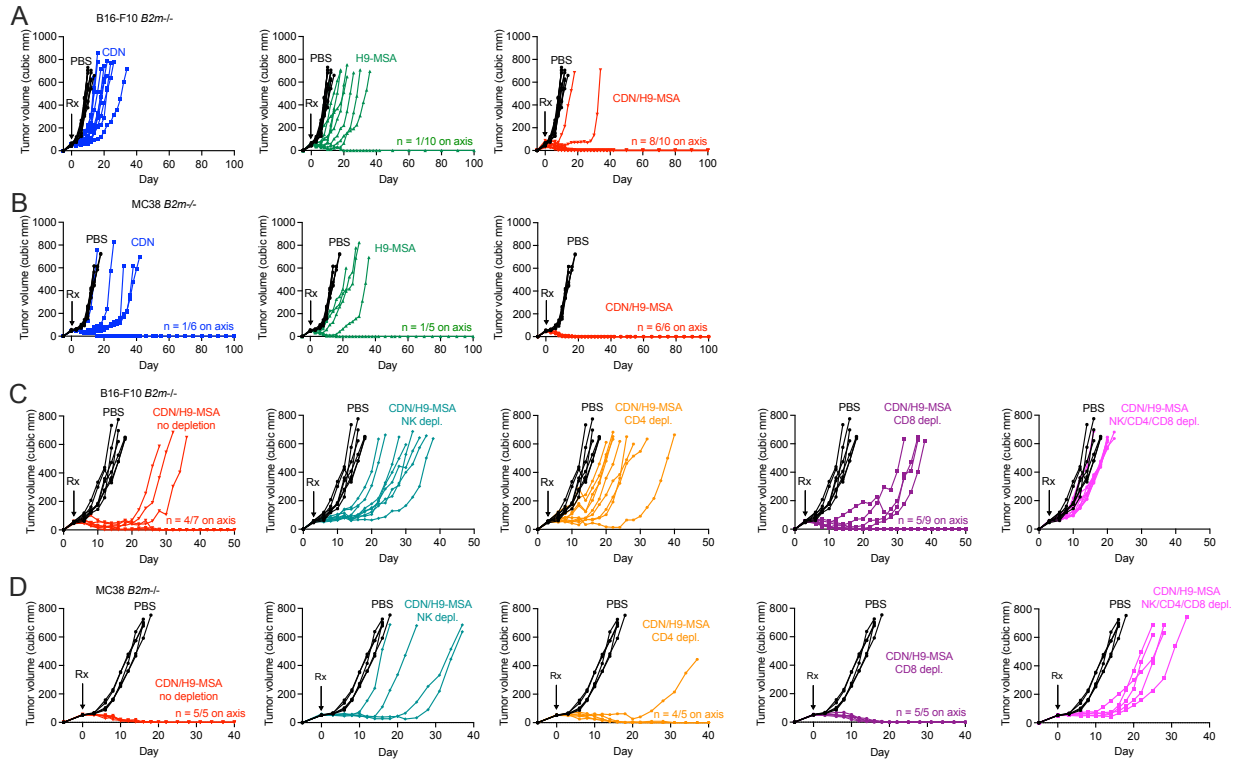
Figure S2. Spider plots showing growth of individual tumors from Figure 1. **(A, C)** B16-F10 *B2m*-/- tumors **(B, D)** MC38 *B2m*-/- tumors. **(A, B)** impact of combination therapy vs monotherapies. **(C, D)** Impact of cellular depletions on the efficacy of CDN/H9-MSA combination therapy.
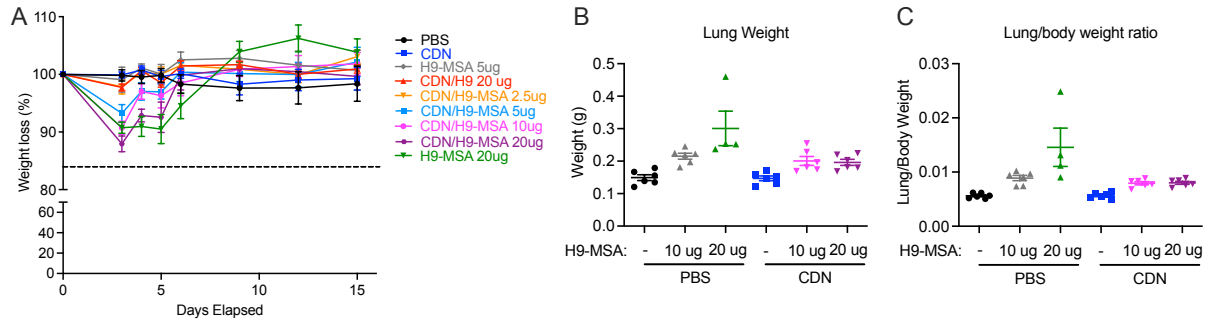
Figure S3. Toxicity associated with H9-MSA or combination therapy. Tumors were generated and mice received therapy as described in Figure S1, legend. Mice were weighed on the indicated days after initiating therapy (d0). In a separated experiment, lungs were harvested on day 6, and wet weights were determined. **(A)** Percentages of d0 body weights over time. **(B)** Lung weight (grams) on day 6. **(C)** The lung/body weight ratio, a measure of pulmonary edema, is shown for each mouse on day 6. Each analysis was confirmed in a repeat experiment.
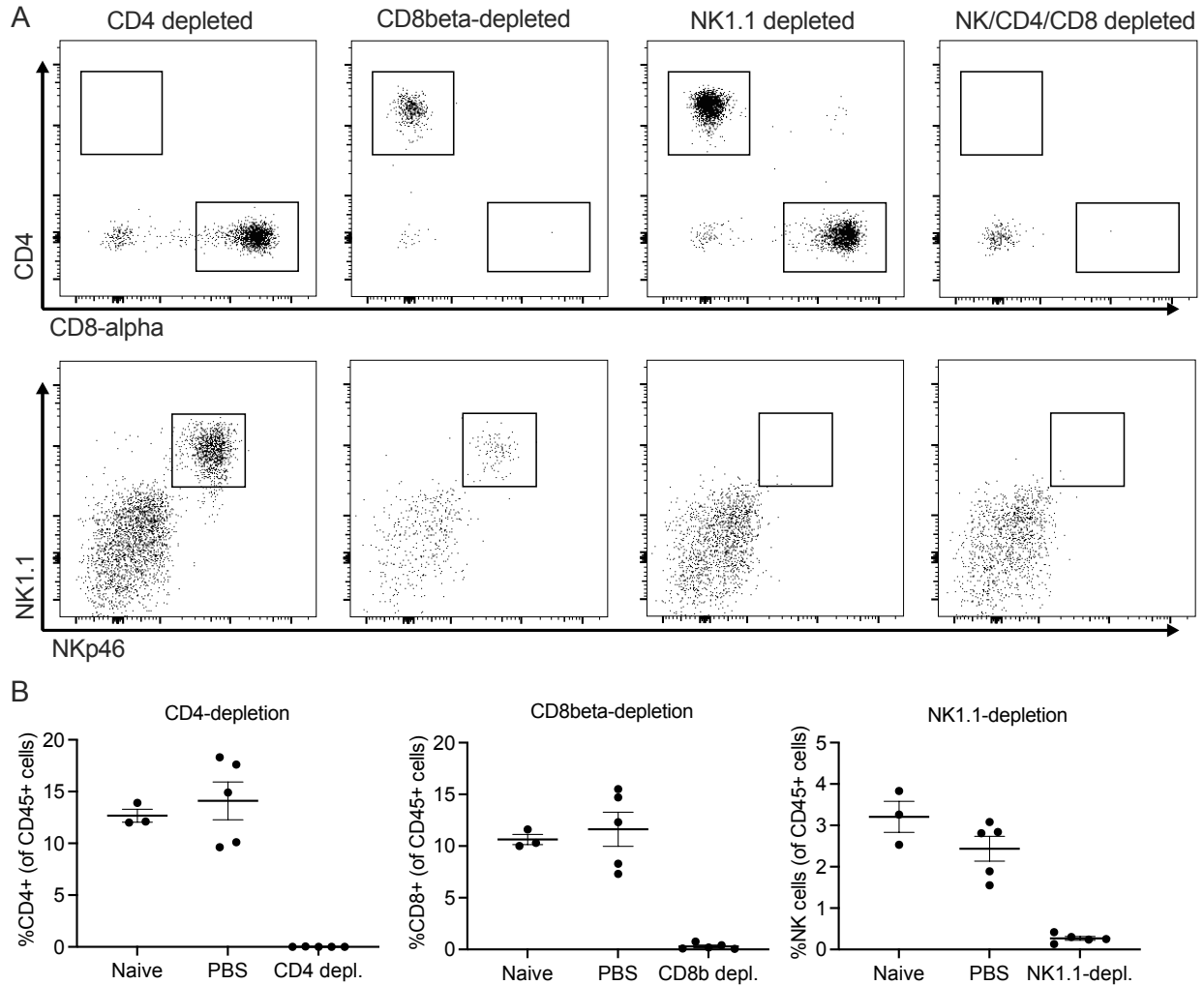
Figure S4. Verification of *in vivo* cellular depletions. (A) Successful T cell and NK cell depletion protocols. As described in Methods, mice were treated on days -2 and -1 with antibodies to deplete CD4+ cells, CD8β+ cells, NK1.1+ cells or all three. On day 0, blood cells were collected, ACK-treated. Gated viable, CD45+, CD19-, Ter119-, F4/80- cells were examined. **(B)** Representative percentages of the indicated cells after the indicated depletions compared to contemporaneous controls.
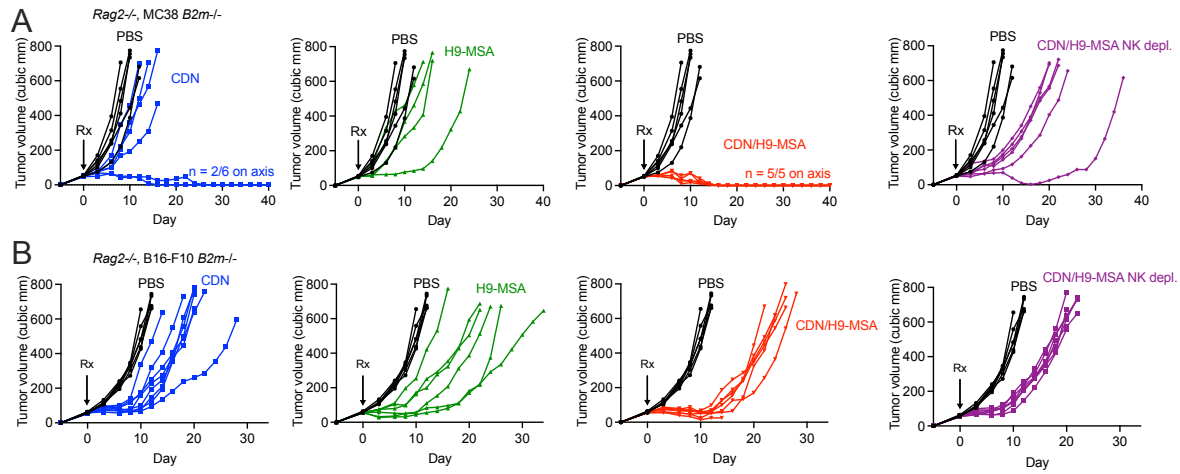
Figure S5: Spider plots showing growth of individual tumors from Figure 2. (A) *Rag2-/-* mice with MC38 *B2m*-/- tumors. **(B)** *Rag 2-/-* mice with B16-F10 *B2m*-/- tumors.
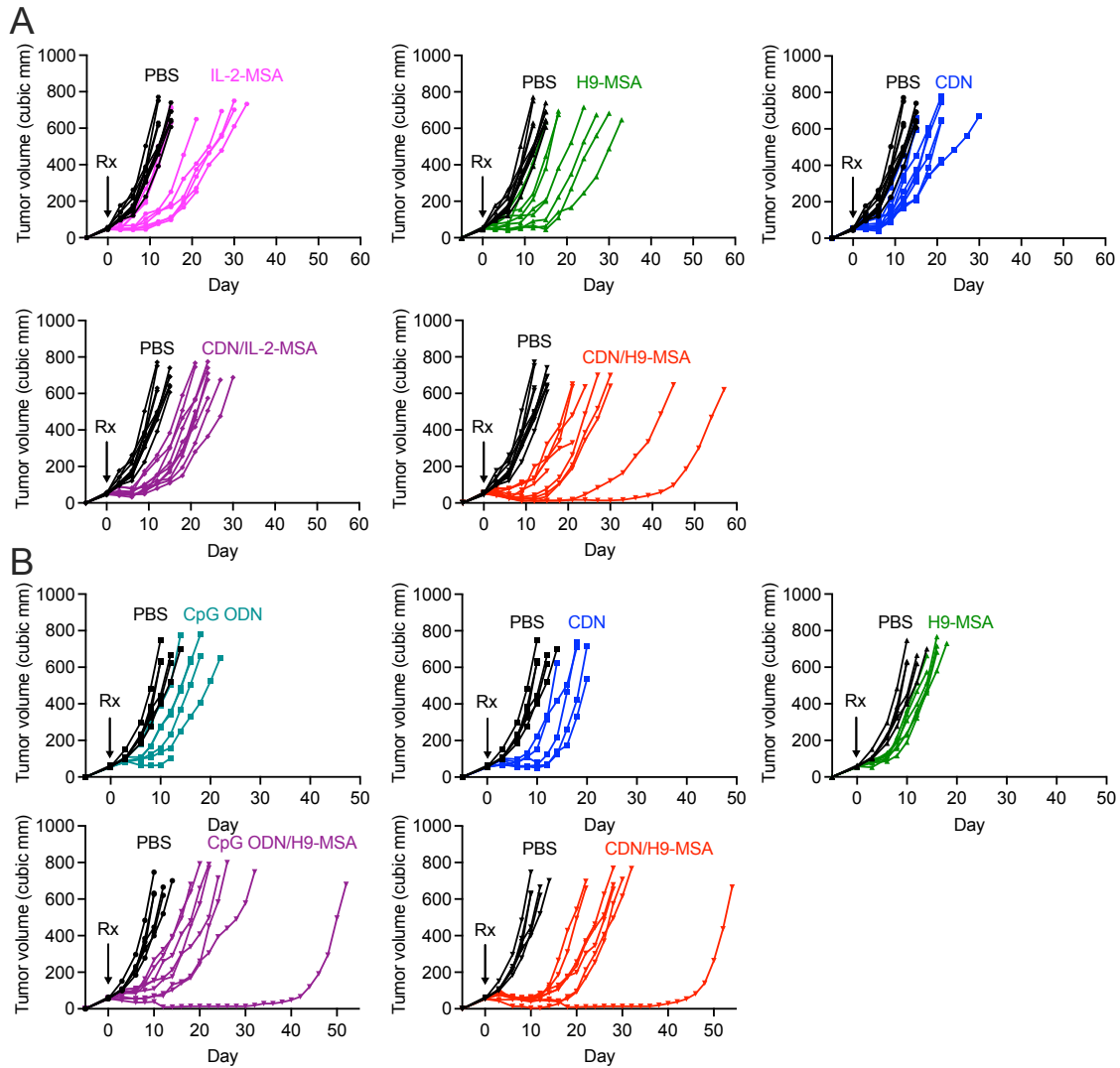
Figure S6: Spider plots showing growth of individual tumors from Figure 4. (A) Spider plots for comparison of IL-2-MSA and H9-MSA treatments. **(B)** Spider plots for comparison of CpG ODN and CDN combination treatments.
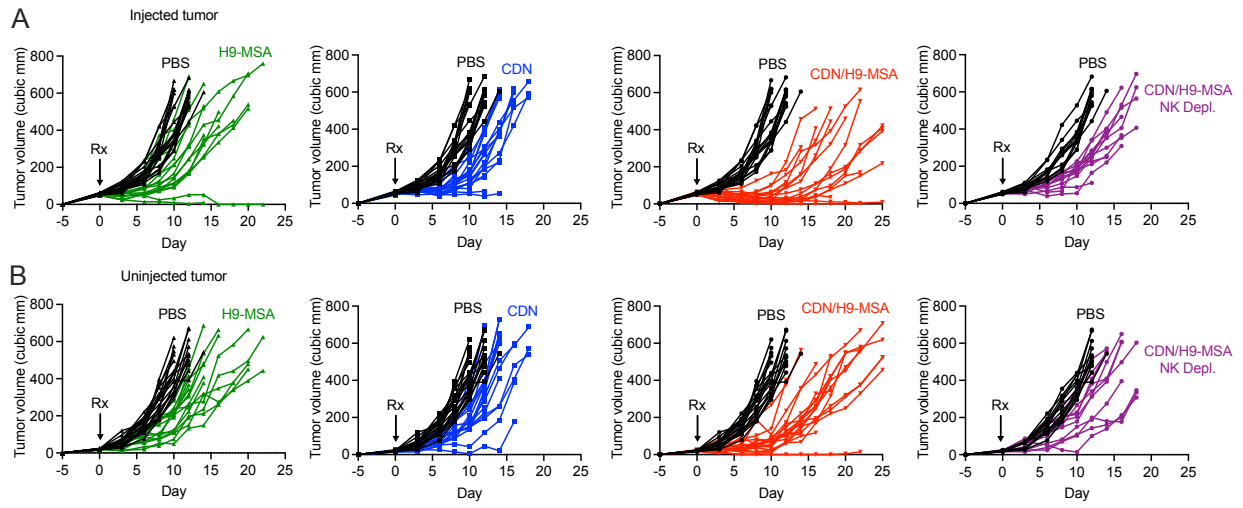
Figure S7: Spider plots showing growth of individual tumors from Figure 5. (A) Injected tumors and **(B)** Uninjected tumors from Fig. 4.
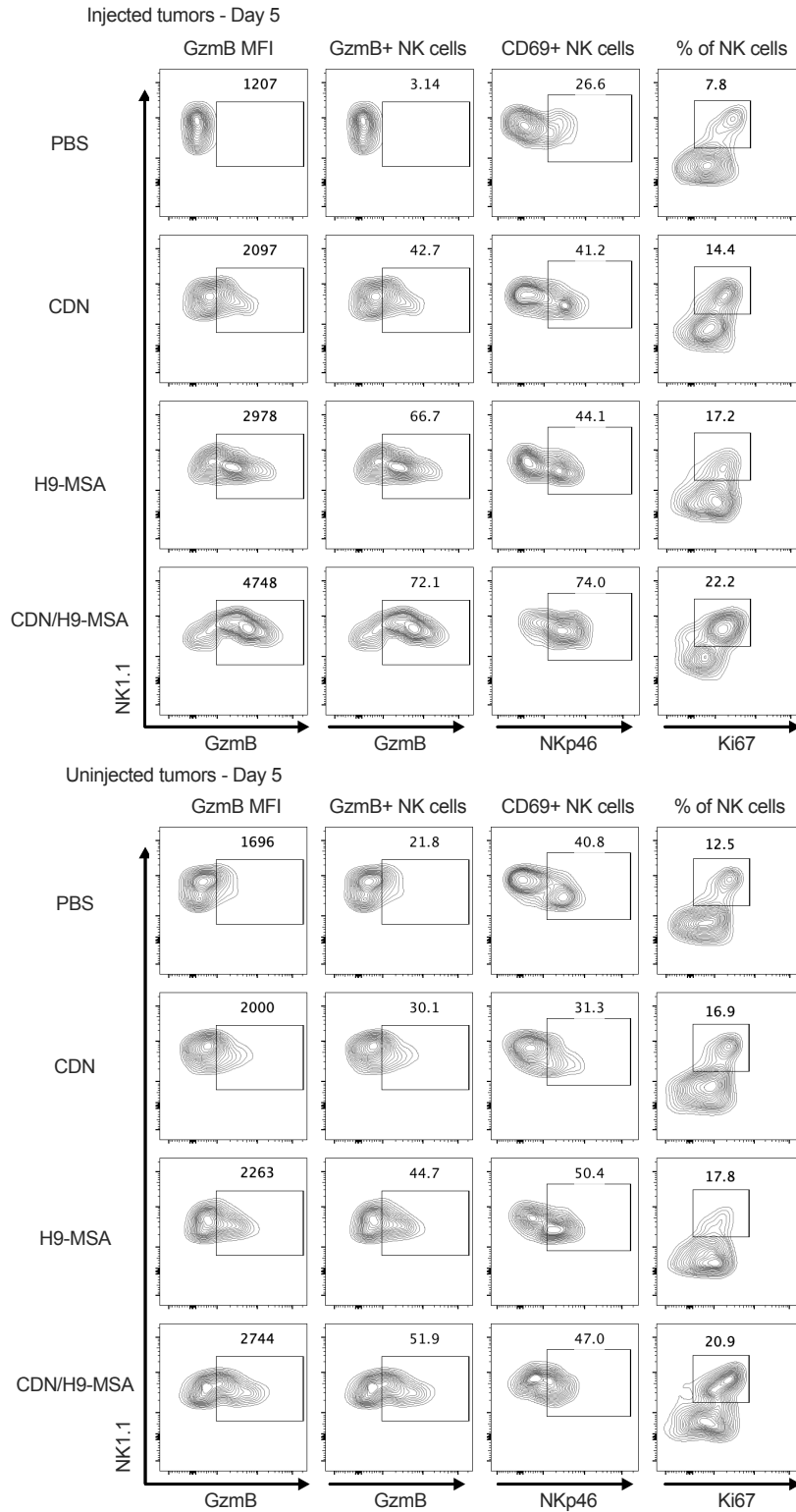
Figure S8: Representative gating strategies for flow cytometry data in Figure 6A. NK cells were gated as viable, CD45$^+$, CD3$^-$, CD19$^-$, F4/80$^-$, Ter119$^-$, NK1.1$^+$, NKp46$^+$ cells.
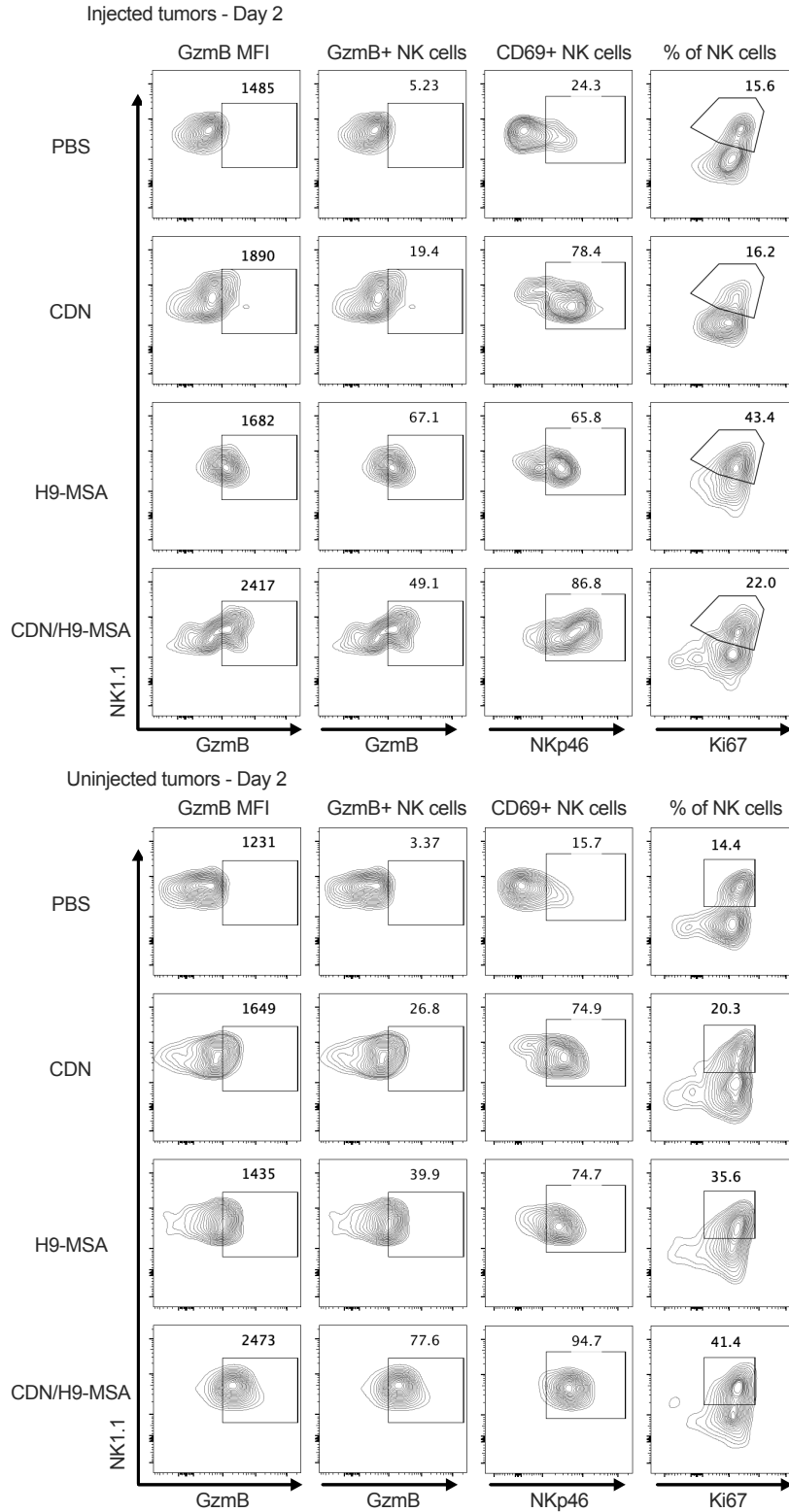
Figure S9: Representative gating strategies for flow cytometry data in Figure 6B. NK cells were gated as viable, CD45^{+}, CD3^{-}, CD19^{-}, F4/80^{-}, Ter119^{-}, NK1.1^{+}, NKp46^{+} cells
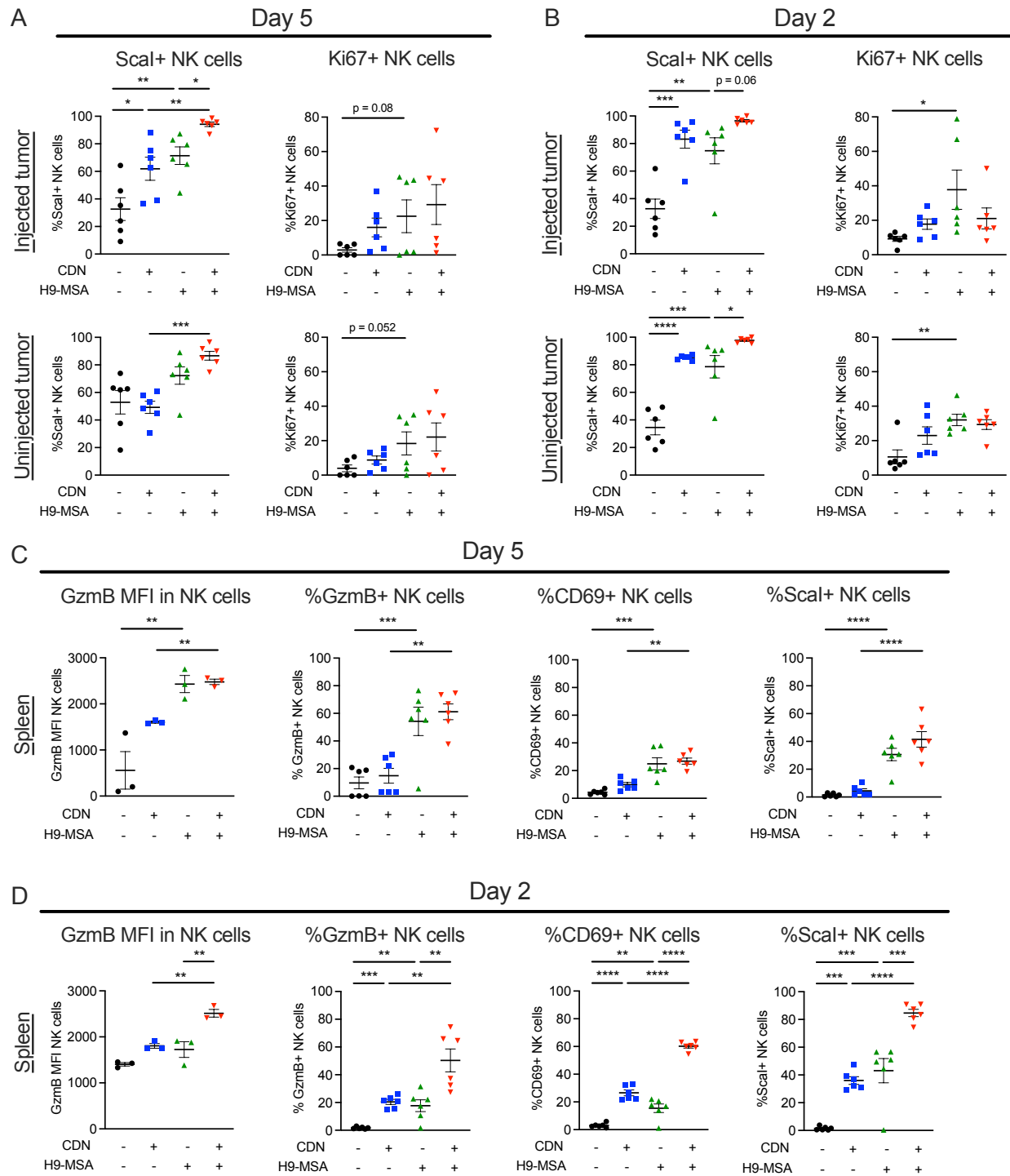
Figure S10: Induction of NK cell activation markers by CDN/H9-MSA treatments in tumors and spleens of mice. B16-F10 *B2m*-/- tumors were established on both flanks of C57BL/6J mice, treated and analyzed as in Figure 5. On d5 **(A)** or d2 **(B)** after initiating therapy,

single cell suspension of both tumors were examined for Sca1 and Ki67 expression on NK cells in both injected and uninjected tumors. Splenocytes on d5 (C) or d2 (D) were examined for intracellular or cell surface markers on NK cells after CDN/H9-MSA treatment. NK cells were gated as viable, CD45$^+$, CD3$^-$, CD19$^-$, F4/80$^-$, Ter119$^-$, NK1.1$^+$, NKp46$^+$ cells. GzmB MFI data are representative of at least 2 independent experiments (n=3) and all other data were combined from 2 independent experiments (n=6). Samples were analyzed by one-way ANOVA.
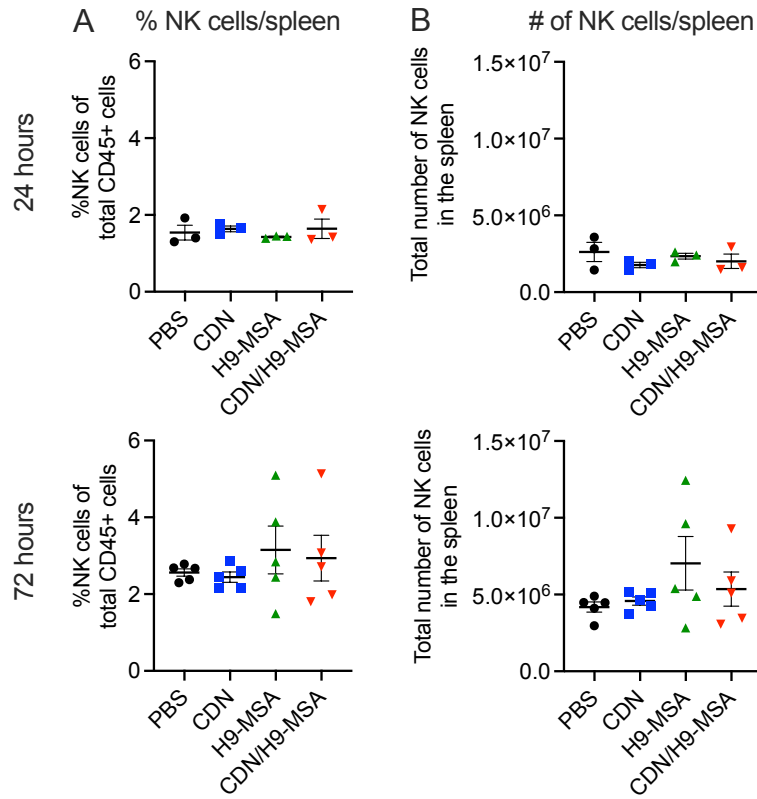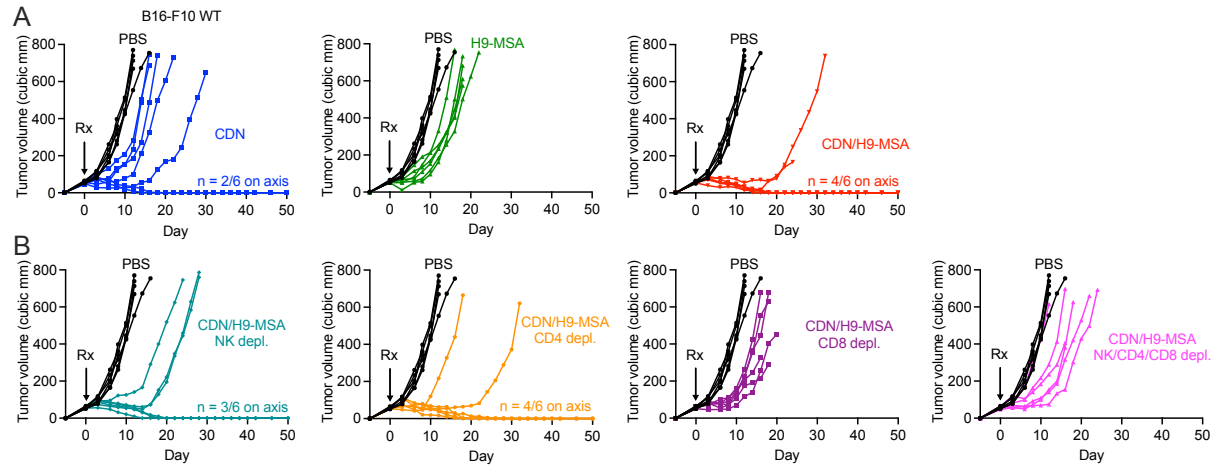
Fig. S11: NK cell percentages and numbers in the spleen after CDN/H9-MSA treatment.

NK cells were gated as viable, CD45$^+$, CD3$^-$, CD19$^-$, F4/80$^-$, Ter119$^-$, NK1.1$^+$ cells. **(A)**

Percentage of NK cells in the spleen. **(B)** Total number of NK cells in the spleen.

Figure S12: Spider plots showing growth of individual tumors from Figure 7. (A) B16-F10 WT tumors and **(B)** B16-F10 WT tumors subjected to cellular depletions.
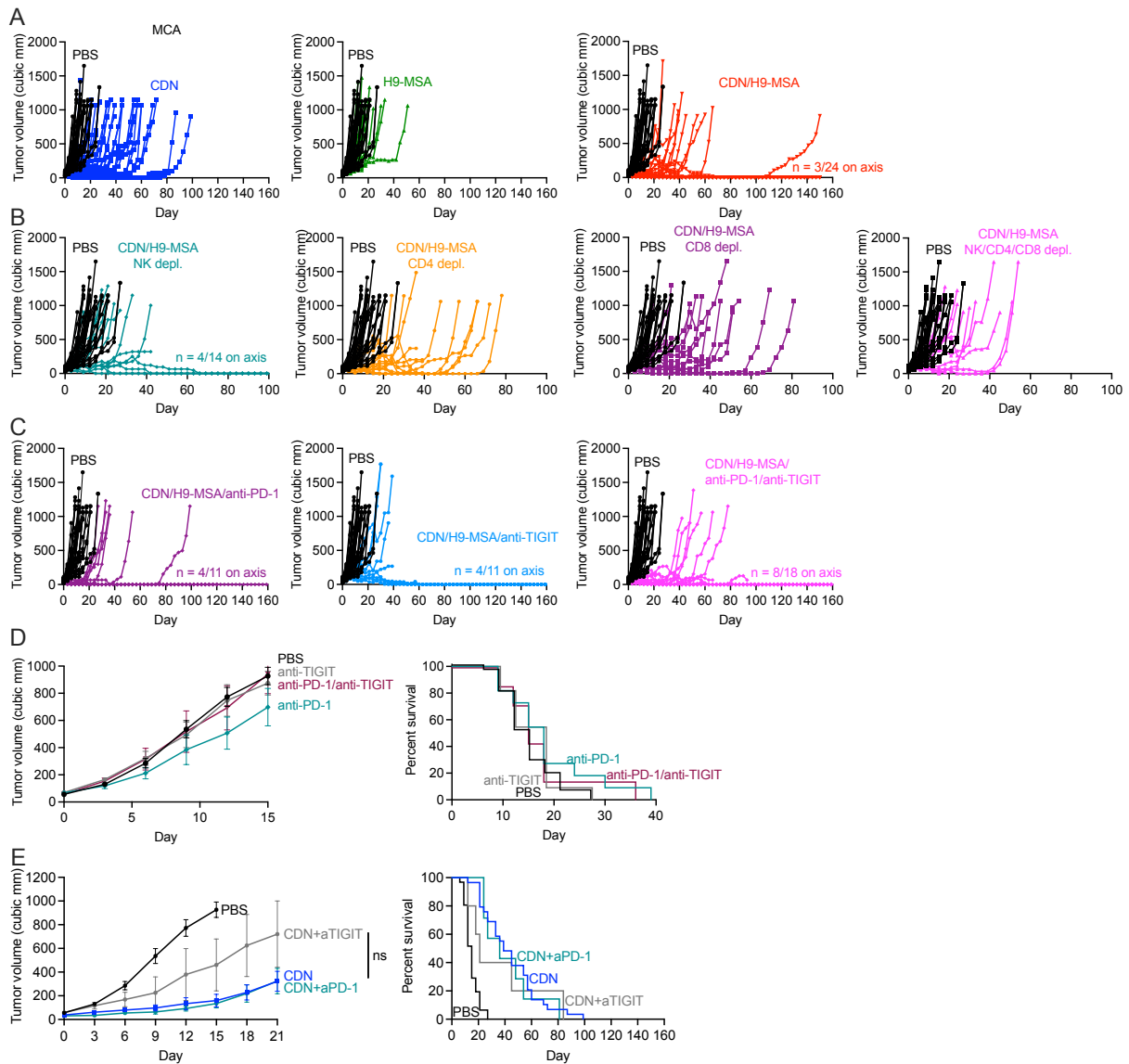
Figure S13: Combination immunotherapy for treating primary sarcomas induced by the carcinogen methylcholanthrene. (A) Spider plots showing individual tumor growth for treated MCA induced tumors from Fig. 7D. **(B)** Spider plots for depletions of MCA induced tumors from Fig. 7E. **(C)** Spider plots for CDN/H9-MSA+checkpoint inhibitor combinations from Fig. 6E. **(D, E)** Tumor averages for single agent checkpoint inhibitors **(D)** or checkpoint inhibitors in combination with CDN **(E)**. The anti-TIGIT antibody employed in these panels was clone 1G9 (BioXCell).